nature energy

REVIEW ARTICLE

https://doi.org/10.1038/s41560-020-00714-4



# Progress and prospects for ultrathin solar cells

Inès Massiot[1], Andrea Cattoni[2,3] and Stéphane Collin[2,3] ✉

**Ultrathin solar cells with thicknesses at least 10 times lower than conventional solar cells could have the unique potential to efficiently convert solar energy into electricity while enabling material savings, shorter deposition times and improved carrier collection in defective absorber materials. Efficient light absorption and hence high power conversion efficiency could be retained in ultrathin absorbers using light-trapping structures that enhance the optical path. Nevertheless, several technical challenges prevent the realization of a practical device. Here we review the state-of-the-art of c-Si, GaAs and Cu(In,Ga)(S,Se)$_2$ ultrathin solar cells and compare their optical performances against theoretical light-trapping models. We then address challenges in the fabrication of ultrathin absorber layers and in nanoscale patterning of light-trapping structures and discuss strategies to ensure efficient charge collection. Finally, we propose practical architectures for ultrathin solar cells that combine photonic and electrical constraints, and identify future research directions and potential applications of ultrathin photovoltaic technologies.**

The share of photovoltaics in renewable energy production is expected to grow from 6.6% in 2017 to 21.8% in 2030[1]. Reaching this target requires not only increases in solar cell efficiencies but also reduction in their cost. The efficiency of single-junction solar cells based on monocrystalline semiconductors is now close to the theoretical Shockley–Queisser (SQ) limit. With respect to a SQ limit of 33.5%[2], GaAs solar cells achieved a 29.1% efficiency with a 1–2-µm-thick absorber layer[3,4]. The indirect bandgap of crystalline silicon (c-Si) is responsible for Auger recombination and much weaker light absorption, which results in a lower theoretical efficiency limit of 29.4%[5] and a record of 26.7% for 165-µm-thick silicon solar cells[6]. The efficiency of polycrystalline solar cells, instead, is still far from the theoretical SQ limit due to lower material quality. Efficiencies of about 23% have been demonstrated for CdTe and Cu(In,Ga)(S,Se)$_2$ (CIGS) semiconductors with 2–4-µm-thick absorber layers[4,7].

In all these solar cells, relatively thick absorbers have been used to ensure that most incident photons are absorbed in a single pass through the cell. However, the effective optical path length can be increased several times by trapping light in the absorber, so that the same values of photogenerated currents and efficiencies can be preserved in much thinner solar cells[8]. With efficient light-trapping strategies, the thickness of solar cells could be reduced by more than one order of magnitude. We refer to ultrathin solar cells as a 10-fold decrease in absorber thickness with respect to conventional solar cells, corresponding to thicknesses below 20 µm for c-Si and 400 nm for thin films such as GaAs, CdTe and CIGS.

Numerous benefits are expected from thinner cells. Reducing material consumption is a direct source of cost reduction in the case of scarce elements (for example, tellurium in CdTe, indium in CIGS and III–V semiconductors). The decrease of deposition times associated with thinner layers directly translates into an increase of the industrial production throughput and lower capital investment costs. From a device perspective, in the case of ultrathin solar cells limited by radiative (GaAs), Auger (Si) or other bulk recombinations (CIGS, CdTe), the open-circuit voltage increases with reduced absorber thickness[8–10]. The carrier collection is also improved in high defect density materials with limited diffusion lengths (CIGS, CdTe). For silicon solar cells, thinning silicon wafers from 160 µm to 50 µm could reduce both manufacturing cost and capex[11]. Beyond, efficiency limits above 28.5% are predicted for thicknesses as low as 10 µm[8,12]. With such thin silicon thicknesses, low-cost chemical vapour deposition (CVD) becomes an appealing deposition technique, combining high throughput and low material consumption[13].

Many light-trapping structures were first implemented in amorphous or microcrystalline silicon solar cells[14] and contributed to the development of concepts that are now applied to more efficient devices. Likewise, the simple fabrication processes of emerging technologies, such as perovskites, organic photovoltaics or colloidal quantum dot solar cells, facilitate the implementation of light-trapping strategies such as plasmonics[15] or photonic crystals[16]. However, most efforts in these fields have been dedicated to material and stability issues rather than advanced light trapping and thickness reduction[17].

So far, most research on ultrathin solar cells has been focused on developing advanced light-trapping strategies based on patterning techniques at the nanometre scale. Assuming Lambertian light trapping, state-of-the-art efficiencies (c-Si, $\eta > 26\%$; GaAs, $\eta > 29\%$; CIGS, $\eta > 23\%$) could be reached for 10-µm-thick c-Si solar cells and 100-nm-thick GaAs or CIGS thin films. However, downscaling the absorber layer thickness challenges the whole design of solar cell architectures. For instance, a longer optical path could increase parasitic absorption in contact layers that do not contribute to photogenerated carriers collected in the device. Texturation of the absorber may also increase non-radiative surface recombination. Overall, the issues of carrier photogeneration and collection are deeply interconnected and thinning the absorber further constrains the realization of selective contacts and passivation layers. Fulfilling the potential of ultrathin solar cells thus requires a comprehensive understanding of the issues limiting the performances of current works.

Here we provide a critical overview of recent advances in ultrathin solar cells based on industrially mature technologies (c-Si, GaAs, CIGS). We discuss generic approaches that can be applied to emerging technologies or to thin films made of CdTe[18] or kesterites[19], for which a thickness reduction has been less explored. In order to highlight the potential in thickness reduction, we first

[1]Laboratoire d'Analyse et d'Architecture des Systèmes (LAAS-CNRS), Université de Toulouse, CNRS, Toulouse, France. [2]Centre de Nanosciences et de Nanotechnologies (C2N), CNRS UMR 9001, Université Paris-Saclay, Palaiseau, France. [3]Institut Photovoltaïque d'Ile-de-France (IPVF), CNRS UMR 9006, Palaiseau, France. ✉e-mail: stephane.collin@c2n.upsaclay.fr

**Box 1 | Light trapping in solar cells**

Absorption in a semiconductor layer is primarily determined by its intrinsic material properties (complex refractive index $n+i\kappa$) and thickness $d$. The absorption coefficient $\alpha = 4\pi\kappa/\lambda$ is strongly material- and wavelength-dependent. Panel a illustrates the difference in behaviour of direct (GaAs, CIGS) and indirect (c-Si) bandgap semiconductors, and the steep decrease of $\alpha$ close to the bandgap. The refractive indices are provided in the Supplementary Data for GaAs and CIGS, and taken from literature for crystalline silicon[185]. Additional coatings, back mirror and texturation can affect the way light enters the cell, propagates, scatters, is trapped and resonates in the absorber, and counterbalance the low absorption in a given wavelength range. The optical path enhancement factor $F$ can be used as a figure-of-merit for the efficiency of light trapping within a solar cell. Absorption at each wavelength is then expressed as $A(\lambda) = 1-e^{-F\alpha d}$.

In the following, we consider three light-trapping models as references to analyse the performances of ultrathin solar cells. The corresponding reference absorption spectra are plotted for a 2-µm-thick slab of c-Si in panel b. For single-pass absorption (panel c), we assume a perfect ARC with no backside reflection: $F$=1. Adding a perfect back reflector leads to double-pass absorption (panel d), and $F = 2$. Light scattering on a sub-wavelength texture (panel e) is the most common way to increase the optical path length in the absorber. It is accomplished through random texturation of the surface or via nanoparticle ensembles. The maximum optical path enhancement factor $F$ requires Lambertian scatterers with perfect ARC and a back mirror[186]. Under these conditions, full randomization of light ray directions and internal reflections result in the Lambertian scattering model, which is described more accurately by $A(\lambda) = \frac{\alpha d}{\alpha d+1/F}$ and $F = 4n^2$ (ref. [187]). For inorganic semiconductors, $F \approx 50$. The remarkable absorption enhancement that can be achieved theoretically with Lambertian light trapping compared to single-pass and double-pass absorption is highlighted in panel b. Periodic patterning has also been investigated as an alternative for light absorption enhancement (panel f). Recent theoretical works suggest that multi-resonant absorption can exceed the absorption enhancement enabled by Lambertian scattering[188,189] but no general model setting the theoretical upper limit for light trapping is available yet.

These light-trapping strategies require texturation or nanostructures at the vicinity of the absorber. Alternatively, external texturation using microtextured foils[190] or imprint-textured glass superstrates[191] can contribute to light management in planar or textured absorbers. In both cases, they result not only in enhanced absorption but also in photon recycling effects induced by light trapping[9] or angular selectivity[192,193]. The concepts of external texturation and angular restriction have not been applied to ultrathin solar cells yet.

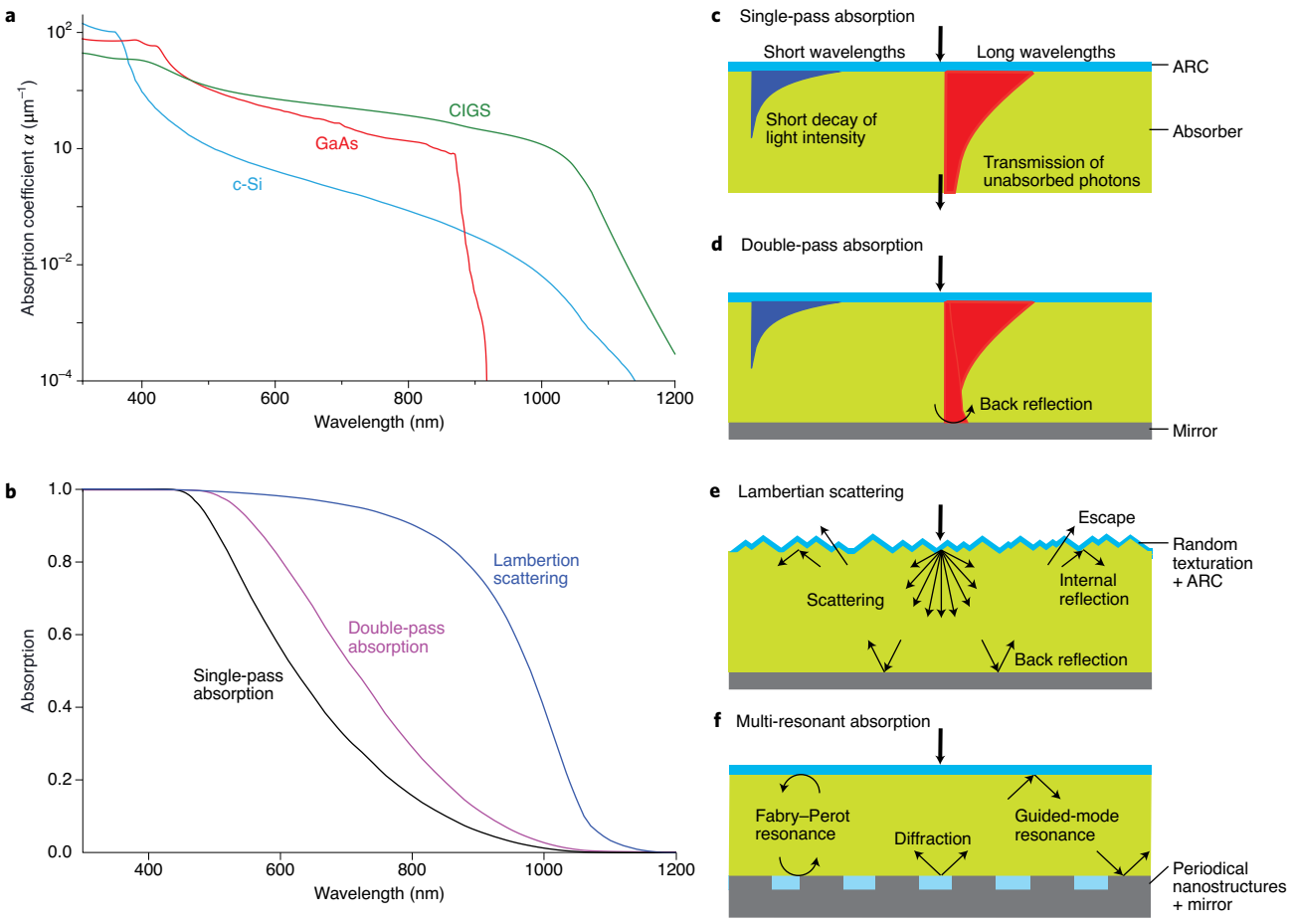

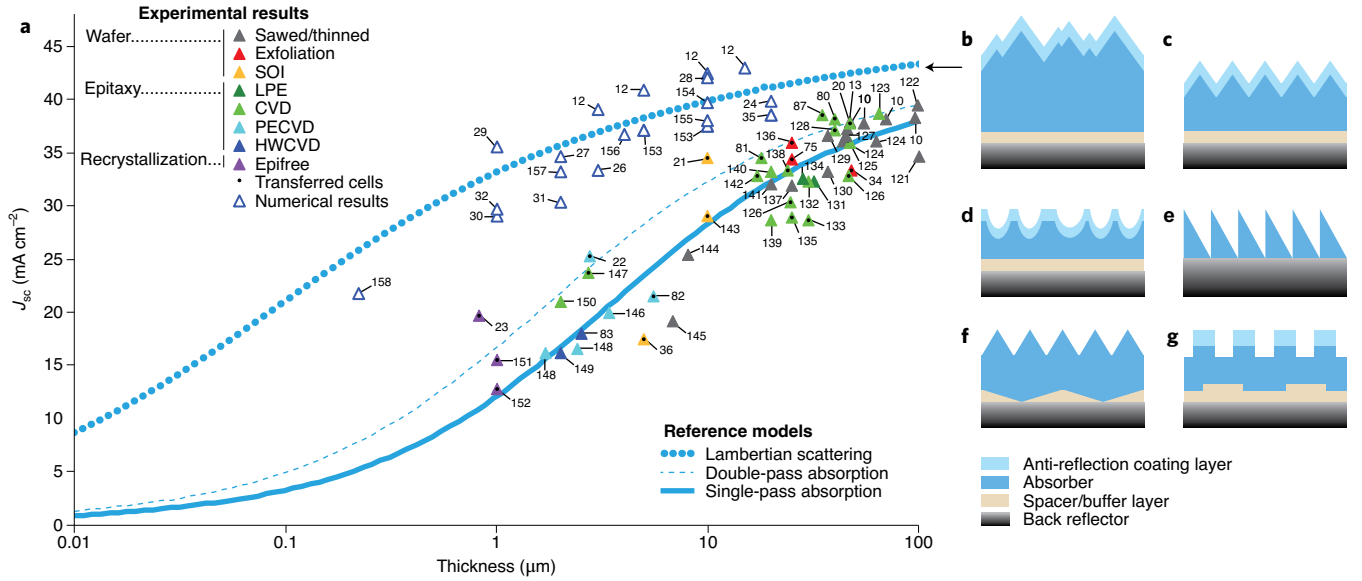


**Fig. 1 | State-of-the-art of ultrathin monocrystalline Si solar cells. a**, $J_{sc}$ of thin (20 μm ≤ $t$ ≤ 100 μm) and ultrathin (<20 μm) c-Si solar cells as a function of the absorber thickness[10,12,13,20–24,26–32,34–36,75,80–83,87,121–158]. Experimental results are indicated with filled coloured triangles and grouped according to the crystal growth method (from Si wafers, epitaxy or recrystallization). HWCVD, hot-wire chemical vapour deposition. The use of a layer transfer process is shown with a black dot. $J_{sc}$ values from numerical calculations and absorption measurements are indicated with open triangles. All reported values are compared to the reference models defined in Box 1 (curves). The $J_{sc}$ value of the record-efficiency c-Si solar cell is indicated by an arrow[6]. **b**–**g**, Sketches of notable light-trapping schemes used in state-of-the-art thin and ultrathin c-Si cells: micrometre-scale random pyramids[10,20,121–126,122] (**b**), front inverted nanopyramid arrays[21,22] (**c**), amorphous ordered nanopatterning[23] (**d**), slanted cones[29] (**e**), front and back nanocone arrays[27] (**f**) and photonic crystals[31] (**g**).

review the progress made in trapping light in ultrathin layers, including numerical works and experimental demonstrations, and we analyse the gap between current optical performances and reference models. We then discuss advances and challenges in the fabrication of ultrathin absorber layers and nanoscale texturation for light trapping. Subsequently, we focus on the most promising strategies to ensure efficient charge carrier collection in ultrathin devices, tackling key issues of surface passivation and carrier selectivity. Finally, we present envisioned architectures for ultrathin solar cells, integrating both aspects of light absorption and charge carrier collection, and we draw conclusions on future directions for research and applications of ultrathin solar cell technologies.

## Benchmarking optical performance of ultrathin solar cells

Light absorption is strongly wavelength dependent and drops with decreasing absorber thickness. For example, less than 40% of photons are absorbed in a single pass above $\lambda = 650$ nm for a 2-μm-thick c-Si solar cell. Enhancing light absorption in the long wavelength range (close to the bandgap) is thus critical to ensure good conversion efficiency in ultrathin solar cells.

Box 1 introduces the concept of light trapping and presents three reference models that we use to analyse the performances of ultrathin c-Si, GaAs and CIGS solar cells: single-pass absorption, double-pass absorption and Lambertian scattering. In order to compare light-trapping efficiencies, we plot the short-circuit current density $J_{sc}$ as a function of the absorber thickness. $J_{sc}$ is the measure of the number of photogenerated carriers collected in the device under sunlight illumination. Assuming a perfect collection of photogenerated carriers, the absorption efficiency is equal to the external quantum efficiency (EQE) and the short-circuit current is given by $J_{SC} = q \int EQE(\lambda) \times \phi_{AM1.5G}(\lambda) d\lambda$, where $q$ is the electronic charge and $\phi_{AM1.5G}(\lambda)$ is the spectral photon flux of the AM1.5G solar spectrum. The thickness considered in the benchmark of ultrathin solar cells is that of the absorber. Window, buffer and back surface field layers, as wide bandgap semiconductors in heterojunctions, are not taken into account. In the case of structured absorbers (textured surfaces, nanowires, and so on), we use the equivalent thickness of a planar absorber with the same volume.

We restrict this Review to single-junction solar cells measured under the standard AM1.5G solar illumination. Since most studies of ultrathin solar cells are still in their infancy, this benchmark is not restricted to solar cells independently measured by a recognized test centre. We report only on solar cells with an area ≥1 mm$^2$, with the exception of ultrathin GaAs solar cells, which have surface areas down to 300 x 300 μm$^2$. The complete data set used in the analysis is provided in the Supplementary Data.

**Ultrathin c-Si solar cells.** Most of the experimental $J_{sc}$ values for state-of-the-art c-Si solar cells lie close to the single-pass absorption reference curve (Fig. 1). Interestingly, the different fabrication processes are clustered in specific thickness ranges. Solar cells thicker than 10 μm are typically fabricated by liquid phase epitaxy (LPE), CVD, or exfoliated from a silicon wafer. For these absorber thicknesses, the light-trapping strategies are limited to the combination of an anti-reflection coating (ARC) and a front texturation made of micrometre-scale random pyramids, as conventionally used for wafer-based silicon cells. Best short-circuit currents reach $J_{sc}$ = 37.9 mA cm$^{-2}$ for 47-μm-thick solar cells[13,20]. As the c-Si thickness decreases, there is a clear increase in the complexity of the strategies used to enhance light absorption. Solar cells thinner than 10 μm require specific fabrication techniques for the absorber layer (epitaxial growth, recrystallization, layer transfer) and submicrometre texturation with novel geometries.

In the sub-10-μm range, three noticeable experimental works have demonstrated a short-circuit current density exceeding double-pass absorption[21–23]. Their common light-trapping strategy is based on the use of a submicrometre front texturing of silicon coupled with a metal back reflector.

A short-circuit current of 34.5 mA cm$^{-2}$ has been achieved with 10-μm-thick silicon solar cells[21]. The light-trapping scheme

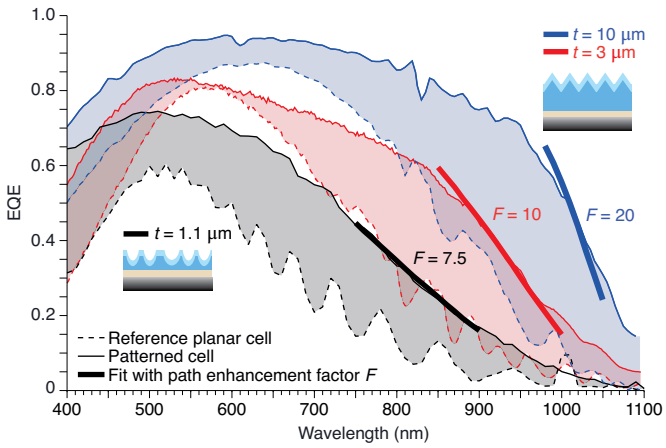


**Fig. 2 | Light-trapping performances of notable ultrathin monocrystalline Si solar cells.** EQE experimental data of patterned ultrathin c-Si solar cells with a nominal thickness $t = 10$ µm (ref. [21]) (solid blue curve), 3 µm (ref. [22]) (solid red curve) and 1.1 µm (ref. [23]) (solid black curve). The EQE data for planar cells with the same thickness are shown as a reference (dashed lines). The filled regions represent the EQE enhancement induced by texturation. The thick plain lines show the fit of the EQE curves in the long wavelength region with the Lambertian model for the following values of $F$ and the equivalent thickness: $F = 20$ and $d_{eq} = 9.83$ µm (ref. [21]), $F = 10$ and $d_{eq} = 2.75$ µm (ref. [22]), and $F = 7.5$ and $d_{eq} = 0.830$ µm (ref. [23]).

integrates a two-dimensional (2D) periodic array of inverted pyramids coated with a silicon nitride layer on the front side and an aluminium back mirror. This proof-of-concept device was fabricated using relatively expensive silicon-on-insulator (SOI) wafers and resulted in high conversion efficiency ($\eta = 15.7\%$).

The same light-trapping strategy with a silver back mirror implemented in a 3-µm-thick Si solar cell led to a short-circuit current density of 25.3 mA cm$^{-2}$ (equivalent thickness of c-Si of 2.75 µm) but an efficiency of only 5% limited by parasitic absorption and surface recombination[22]. In this case though, the c-Si layer was epitaxially grown by low-temperature plasma-enhanced CVD (PECVD) and transferred on a glass substrate via anodic bonding and mechanical cleavage. The front texturing was fabricated using nanoimprint lithography (NIL) and wet etching.

Further thickness reduction led to a certified conversion efficiency of 8.6% (19.7 mA cm$^{-2}$) for a 1.1 µm-thick c-Si layer produced by the 'epifree' method[23]. As an alternative to periodical pyramid arrays, the front surface of the cell is textured with a short-range ordered arrangement of parabolic holes fabricated by colloidal lithography and dry etching. The significant conversion efficiency obtained for such a thin absorber layer (equivalent thickness of 830 nm) demonstrates that a submicrometre texturing of the absorber by dry etching can be combined with efficient passivation.

The last two approaches combine a bottom-up growth method (PECVD, epifree) with a layer-transfer process for an effective reduction of material use and implement upscalable patterning techniques such as nanoimprint and colloidal lithography[22,23]. Industrially viable ultrathin silicon solar cells could stem from combining the best of these three works, applying bottom-up growth methods and scalable patterning techniques to the processing of 10-µm-thick silicon cells to reach efficiencies above 15%.

The light-trapping efficiency can be quantified by calculating the light path enhancement factor $F$ with respect to a single pass. In the weakly absorbing regime ($\alpha \times d$ tends to zero, where $\alpha$ is the absorption coefficient and $d$ the thickness), the absorption can be approximated by the Lambertian scattering model[22] as expressed in Box 1. Hence $F$ can be estimated for a particular light-trapping strategy by fitting EQE measurements with the Lambertian expression in a restricted wavelength range close to the bandgap. Note that the equivalent thickness of the textured silicon layer should be determined beforehand to be implemented in the Lambertian model. Figure 2 illustrates the determination of light path enhancement factors for periodic[21,22] and disordered[23] front texturations of the silicon layer. In the case of $F = 10$, the light path enhancement has been further decomposed into the combination of the increased effective thickness due to diffraction on the inverted pyramid array (x1.25 enhancement) and the reflection on both the front (x4) and back (x2) interfaces[22].

Despite these promising advances, there is still a significant gap between the light-trapping performances of experimental works and the Lambertian model (Fig. 1). Numerical studies using simplified cell designs explored novel geometries, from inverted pyramids[12,24] to photonic crystals[25], gratings[26], nanocone arrays[27], slanted cones[28,29] and quasi-random structures[30]. Remarkably, the best numerical performances actually exceed the Lambertian reference using resonant modes in a slanted conical-pore photonic crystal combined with a back silver mirror[28,29]. Because of the simplified cell architecture, the predicted short-circuit currents are likely to be overestimated. Nevertheless, these works give us a hint of the potential gain using properly designed nanophotonic structures. The periodicity plays a key role in the design. Wavelength-scale front structuration can efficiently diffract light into the silicon absorber with negligible diffraction losses in air[21,22] and asymmetry can increase the number of resonances as well as the overall absorption[28,29]. Models that include a complete solar cell structure lead to significantly lower performances[31,32].

Actually, most experimental works are still below the double-pass absorption. Aside from non-perfect antireflection coatings, two main sources of losses should be taken into account in the cell design: losses in contact layers (parasitic absorption and non-radiative recombination) and absorption in the back mirror. Parasitic absorption occurs in transparent conductive oxides (TCO), the highly-doped contacts and the passivating layers, and it is likely to be exacerbated by light trapping[31,32]. Optical losses in the metal reflector are inevitable; in particular for nanostructured mirrors whenever surface plasmon resonances are excited. Losses can be reduced by introducing a thin dielectric layer with a low refractive index between the silicon and the mirror[33,34]. This is normally accomplished in a PERC silicon cell by the $Al_2O_3$/SiN layer also used to define the localized contacts. Alternatively, an omnidirectional distributed Bragg reflector (DBR) with negligible losses can be designed to operate in the relatively narrow region of weak absorption of crystalline silicon. Almost $4n^2$, where $n$ is the refractive index of the material, optical path enhancement has been demonstrated in 28-µm-thick Si using a front texturation coupled with an omnidirectional DBR reflector composed of only 6 pairs of a-Si/SiN layers[35]. When coupled with a back texturation, the DBR should be carefully designed to avoid transmission losses[35,36].

**Ultrathin GaAs solar cells.** With a direct bandgap and a high radiative efficiency[37], GaAs is a model system to explore novel light-trapping strategies that can be applied to other materials. Record single-junction solar cells with efficiency of 29.1% have been achieved with a back mirror that boosted both the $J_{sc}$ (absorption improvement) and the $V_{oc}$ (photon recycling)[3,4]. In ultrathin solar cells, internal losses may still hinder photon recycling[9] while light trapping has been successfully used to improve $J_{sc}$. First attempts based on the use of metal nanoparticles as scatterers led to relatively low $J_{sc}$ due to parasitic absorption and the lack of a back mirror[38,39] (Fig. 3). These drawbacks were circumvented using gold deposited on a rough AlInP layer, acting as both a contact and a scattering back mirror[40], which resulted in $J_{sc} = 24.5$ mA cm$^{-2}$ ($\eta = 19.1\%$)

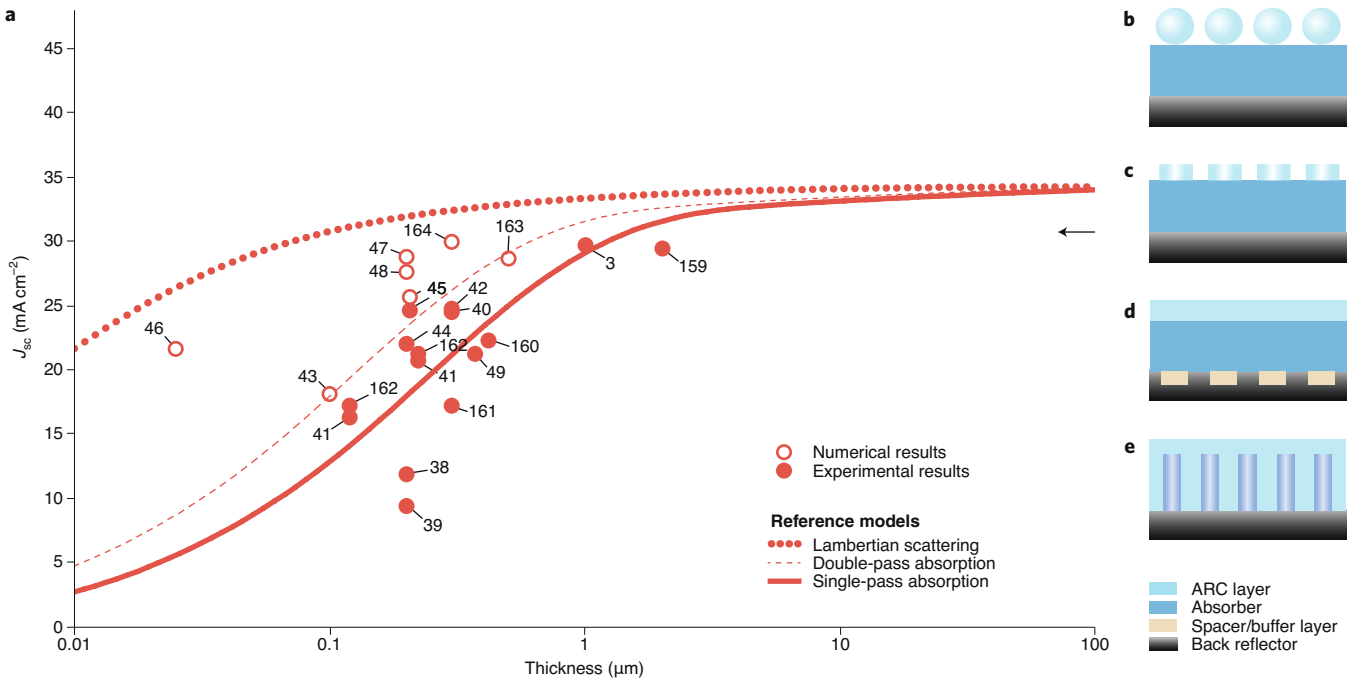


**Fig. 3 | State-of-the-art of ultrathin GaAs solar cells. a**, Short-circuit current density ($J_{sc}$) of thin (>400 nm) and ultrathin (<400 nm) GaAs solar cells as a function of the absorber thickness[3,38–49,159–164]. Experimental results are indicated with filled circles. $J_{sc}$ values from numerical calculations are indicated with open circles. All reported values are compared to the reference models defined in Box 1 (curves). The $J_{sc}$ value of the best-efficiency GaAs solar cell is indicated by an arrow. **b**–**e**, Sketches of notable advanced light-trapping schemes used in state-of-the-art ultrathin GaAs cells: front dielectric nanostructure arrays[43,44] (**b**,**c**), nanostructured back mirror[45] (**d**) and nanowire arrays[49] (**e**).

for a 300-nm-thick GaAs layer[40]. Light trapping and carrier collection can also be optimized separately by combining localized ohmic contacts and a high-reflectivity silver back mirror[41]. This idea was implemented using a rough back mirror fabricated by simple wet chemical etching of an $Al_{0.3}Ga_{0.7}Al$ contact layer and led to an efficiency of 21.4% with $J_{sc} = 24.8$ mA cm$^{-2}$ (ref. [42]).

To further enhance light absorption, most recent approaches rely on periodic arrangements of nanostructures to excite resonant modes. They can be localized in dielectric nanostructures (Mie resonances)[43] or preferably in the active layer by guided-mode resonances[44,45]. In the latter case, diffracted waves induced by the grating couple to waveguide modes. The spectral position and intensity of the resonance peaks can be tuned via the geometry of the nanostructures so that multiple resonances partially overlap leading to broadband absorption enhancement. Using this approach, dielectric nanostructure arrays deposited on the front surface of 200-nm-thick solar cells resulted in $J_{sc} = 22$ mA cm$^{-2}$ ($\eta = 16.2\%$)[44]. An improved $J_{sc}$ of 24.6 mA cm$^{-2}$ was obtained with a nanostructured back mirror fabricated by NIL and combined with localized contacts[45]. The latest result exceeds single-pass absorption by 7 mA cm$^{-2}$, and has led to a certified efficiency of $\eta = 19.9\%$. A detailed loss analysis shows that the same architecture could lead to an efficiency of 25%.

The room left for absorption enhancement is explored by a few numerical studies. For very thin structures (25 nm), metal–semiconductor–metal plasmonic cavities exhibit broadband light absorption while keeping planar active layers[46]. Interestingly, another strategy relies on multi-resonant vertical nanostructures to induce a series of resonances regularly shifted spectrally[47,48]. A value of $J_{sc} = 28.8$ mA cm$^{-2}$ close to the Lambertian scattering model has been predicted with an array of nanocones corresponding to an equivalent thickness of 200 nm[47]. Though the structures proposed to date by these numerical studies are limited to simplified solar cell structures or exotic geometries difficult to fabricate, they can inspire the design of more realistic architectures that may reach or even overcome the performances predicted by the Lambertian scattering model. For now, nanowire-based solar cells are the closest practical example of a three-dimensional approach alternative to thin-film solar cells. They take advantage of a selective epitaxial growth and light-trapping properties intrinsic to the nanowire geometry and led to a record $J_{sc} = 21.4$ mA cm$^{-2}$ demonstrated with axial GaAs p–n junctions (equivalent thickness 370 nm, $\eta = 15.3\%$)[49].

**Ultrathin CIGS solar cells.** Reducing the absorber thickness is a promising way to improve the industrial competitiveness of CIGS photovoltaic modules, thanks to lower material use and an increased throughput[50]. The conventional structure of a CIGS solar cell is made of a CdS/Cu(In,Ga)$Se_2$ heterojunction deposited on a molybdenum (Mo) back contact. Front side collection of electrons is ensured through undoped and Al-doped ZnO window layers coupled with an ARC. Depending on the CIGS composition, its bandgap may slightly vary around 1.15–1.2 eV. CIGS absorbers thinner than 1 μm have led to many experimental and numerical results, as reported in Fig. 4. Remarkably, all the experimental results lie below the single-pass absorption.

This loss in $J_{sc}$ is mainly attributed to parasitic absorption and surface recombination. On the front side, parasitic absorption occurs in the CdS buffer layer at short wavelengths, independent from the absorber thickness. It can be avoided through the use of wider bandgap Zn(O,S)-based buffer layers[7]. On the back side, parasitic absorption in the Mo contact resulting from low reflection at the CIGS/Mo interface occurs at longer wavelengths and its impact increases dramatically for ultrathin CIGS layers[51–59]. Additionally, higher surface recombination is induced in thinner absorbers by carriers photogenerated closer to the back contact[52]. This can be circumvented using thin ($Al_2O_3$, $MgF_2$) passivation layers with nanosized point contacts between CIGS and Mo, resulting in $J_{sc} = 31.1$ mA cm$^{-2}$ ($\eta = 13.5\%$) for 385-nm-thick CIGS absorbers[60], and $J_{sc} = 23.3$ mA cm$^{-2}$ ($\eta = 11.8\%$) for 240-nm-thick CIGS[61].

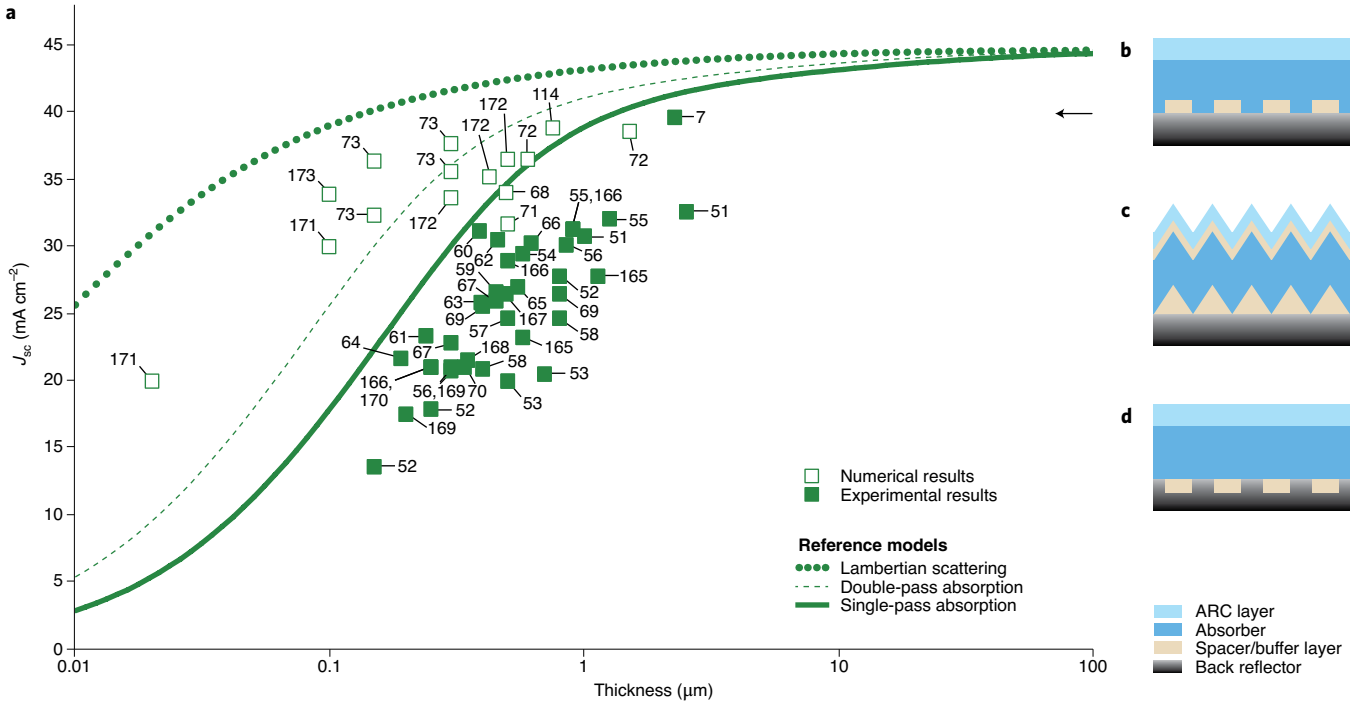


**Fig. 4 | State-of-the-art of ultrathin CIGS solar cells. a**, $J_{sc}$ of thin (>400 nm) and ultrathin (<400 nm) CIGS solar cells as a function of the absorber thickness[7,51–73,165–173]. Experimental results are indicated with filled squares. $J_{sc}$ values from numerical calculations are indicated with open squares. All reported values are compared to the reference models defined in Box 1 (curves). The $J_{sc}$ value of the best-efficiency CIGS solar cell is indicated by an arrow. **b**–**d**, Sketches of notable advanced light-trapping schemes used in state-of-the-art ultrathin CIGS cells: back dielectric nanostructure arrays[64] (**b**), deposition on textured substrates[72] (**c**) and nanostructured back mirror[73] (**d**).

Nanostructured dielectric layers have also been proposed to combine point contacts with increased optical reflectance and scattering at the CIGS/Mo interface. $SiO_2$ nanostructures made by NIL or nanosphere lithography have been introduced in 500-nm-thick CIGS solar cells[59,62,63]. It is worth noting that these devices cannot be directly compared to others due to a lower CIGS bandgap (~1 eV). A $J_{sc}$ of 21.6 mA cm$^{-2}$ ($\eta$ = 9%) was demonstrated with 190-nm-thick CIGS deposited on a nanostructured $SiO_2$ layer fabricated by interference lithography[64]. Still, the light-trapping efficiency of these devices is limited by the low reflectivity of the Mo back contact. The choice of alternative materials (ZrN (ref. [65]),TCO (refs. [66–68])) is constrained by the high temperature of the CIGS deposition process. For this reason, highly reflective metals such as Au (ref. [69]) and Ag (ref. [70]) have only been introduced in a superstrate configuration.

The optical design of light-trapping nanostructures has been hampered by the lack of reliable data for the CIGS refractive index close to the bandgap and by the presence of a composition gradient. Consequently, quantitative comparison between experiments, reference models and numerical results should be handled with caution. Nevertheless, optical modelling has contributed to the assessment of optical losses in actual devices[62–64,67,69,71] and provides guidelines for future designs. The integration of 2D pyramids arrays with a silver back mirror in a 600-nm-thick CIGS solar cell could lead to $J_{sc}$ = 36.4 mA cm$^{-2}$ (ref. [72]). The same $J_{sc}$ has been predicted for only 150 nm of CIGS with a periodically nanostructured silver back mirror[73]. To meet these predictions and unlock the performance of ultrathin CIGS solar cells, the main technological challenge currently pursued by many groups is the development of a back contact able to sustain CIGS deposition temperatures of about 500 °C, provide a high optical reflectivity and form an ohmic contact with CIGS with low surface recombination.

## Fabricating ultrathin absorber layers

The best designs for light trapping consist of a highly reflective back mirror combined with nanostructured front/rear surfaces to couple and guide light in the ultrathin absorber. Making these devices entails tackling two issues that will be discussed in this section: the fabrication of the ultrathin semiconductor layer and its transfer onto a back reflector.

**Ultrathin c-Si solar cells.** The integration of a back mirror requires transfer of a thin film by exfoliation from a thick wafer or by epitaxial growth and subsequent lift-off. The conventional process for producing silicon wafers out of the ingot uses a wire sawing technology. The material removed by the cutting blade (kerf) and wasted, about 40%, is likely to increase for ultrathin solar cells[11].

The first logical evolution of this technology, named kerfless wafering, is based on the mechanical exfoliation of a thin Si film from a thick wafer. The 'spalling' process uses an applied stress to remove a film with a predetermined thickness in the range of a few tens of micrometres (Fig. 5a). The crack tends to follow a trajectory parallel to the film/substrate interface to minimize the shear stress component[74]. This technique has been used for 25-μm-thick c-Si solar cells with 14.9% efficiency[75]. It has also been used for Ge[76] and III–V layers, and no degradation was observed in spalled GaAs solar cells with efficiency of 18.4% and $V_{oc}$ = 1.07 V (ref. [77]). The simplicity of the technique makes it very attractive. However, the feasibility of multiple exfoliations from the same ingot over large surface areas and the precise control of the fracture depth layer thickness remain to be demonstrated.

The 'smart-cut' process provides a way to precisely define the fracture interface at a determined depth from a few tens of nanometres up to about 10 μm by ion implantation (Fig. 5b)[78]. It has been implemented for silicon-on-insulator wafers destined for chip manufacturing and used for proof-of-concept photovoltaic devices

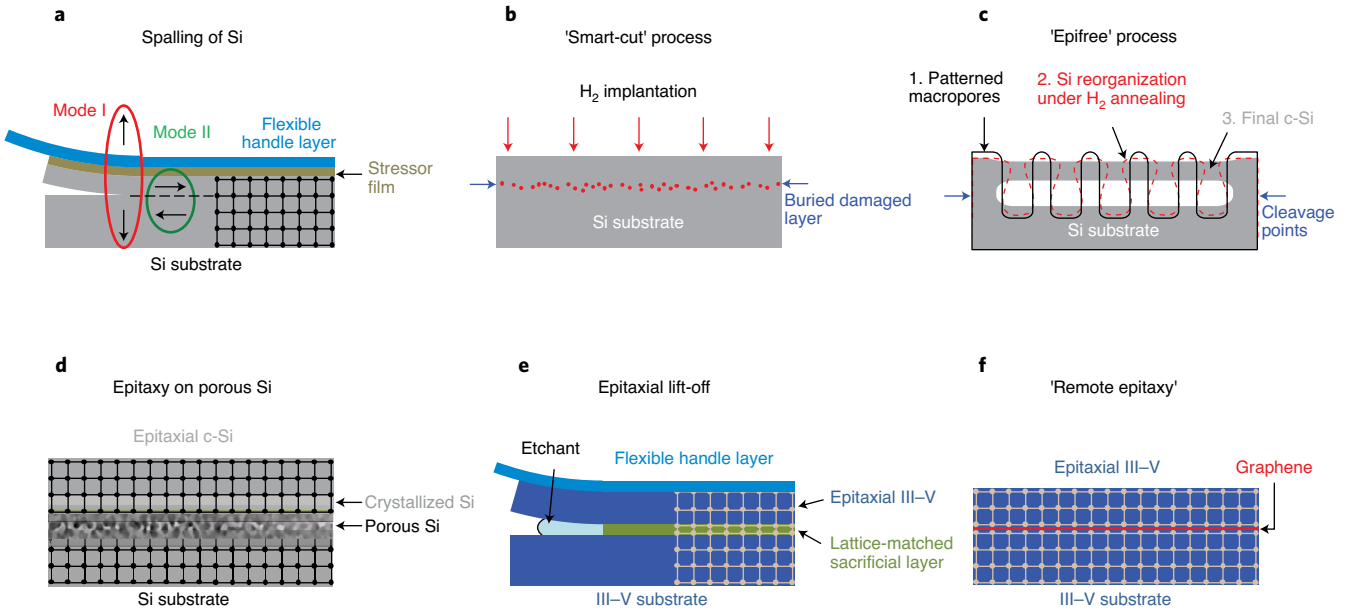


**Fig. 5 | Transfer techniques for monocrystalline semiconductor thin-films. a**, Spalling makes use of a stressor layer (metal or glue) deposited on the silicon wafer, which induces a pure opening stress (mode I) and a shear stress (mode II)[74]. **b**, The 'smart-cut' process is based on ion implantation to create a buried damaged layer at a specific depth[78]. Its expansion upon annealing (400–600 °C) causes the detachment of the top thin silicon film with a relatively low roughness as compared to spalling. **c**, In the epifree process, cylindrical nanopore arrays are first etched in a silicon wafer that is subsequently recrystallized at high temperature (1100 °C) in an inert atmosphere. Reorganization upon annealing results in a single-crystal silicon layer suspended on a void cavity[23]. **d**, A fragile, recrystallized porous layer allows the detachment and transfer of the epitaxially grown silicon layers. **e**, In the epitaxial lift-off of III–V, the peel-off of the absorber layer is accomplished by selectively etching a lattice-matched release layer sandwiched between the epitaxial layer and the substrate[88,89]. **f**, In the remote epitaxy on graphene, the weak van der Waals potential of graphene cannot completely screen atomic interactions with the substrate allowing lattice-matched epitaxy together with easier mechanical release[93].

such as 10-µm-thick c-Si solar cells with 15.7% efficiency[21]. Yet, the viability of this process to fabricate solar cells in a cost-effective way at the industrial scale is questionable.

First introduced as silicon-on-nothing[79], the epifree process (Fig. 5c) is another technique for the mechanical exfoliation of thin Si films, still limited by the maximum thickness achievable (2–3 µm). Record ultrathin c-Si solar cells (8.6%) have been successfully demonstrated using released 1-µm-thick high-quality monocrystalline thin films[23].

Crystalline silicon thin films can also be fabricated by direct epitaxial growth techniques, such as LPE and CVD in various forms. CVD performed at relatively high temperatures offers high deposition rates (~µm $min^{-1}$) and has been widely used in a thickness range from 15 to 50 µm[13,80,81]. For thinner silicon films (1–10 µm), low-temperature PECVD and hot-wire CVD have been developed recently and lead to high-quality layers with a lower thermal budget but also lower growth rates (50–300 nm $min^{-1}$)[82,83]. The introduction of a porous silicon layer prior to the epitaxial growth enables the release of an ultrathin silicon layer or even a complete solar cell (Fig. 5d). The residual porous Si is then removed and the substrate reused for additional growths[84–86]. This technique has led to remarkable $J_{sc}$ values for different thicknesses[13,22,80,81,87].

**Ultrathin GaAs solar cells.** Epitaxial growth is undoubtedly the most extensively used and versatile approach for III–V semiconductors. The main challenge is to cost-effectively transfer the epitaxial layer on a host substrate. Using 'epitaxial lift-off' with an AlAs sacrificial layer[88,89] (Fig. 5e), GaAs layers transferred onto a metallic mirror have led to record single-junction solar cells[3]. Cost reduction is still hindered by the limited number of substrate reuse (about a few tens).

Similarly to the epifree process, a germanium-on-nothing technology has also been developed to fabricate ultrathin single-crystal Ge membranes that can be used for epitaxial growth and transfer of GaAs solar cells[90]. 1-$mm^2$-area processed GaAs cells on a Ge membrane exhibit similar $V_{oc}$ values (0.835 V) as reference cells grown on bulk Ge.

Alternative methods to separate the epitaxial film from the substrate rely on the presence of a fragile interface or a poor adhesion between the template substrate and the epitaxial film. This idea was first implemented in the 'CLEFT' (cleavage of lateral epitaxial films for transfer) process using a graphite mask patterned on a GaAs (110) substrate[91]. Nucleation and epitaxial growth start from the openings, continue by lateral overgrowth and produce a single-crystal GaAs film that can be mechanically cleaved. This technique has not been developed further despite promising 17%-efficient GaAs cells being demonstrated in 1981[92].

More recently, a novel approach named 'remote epitaxy' of thin films on (100) III–V semiconductor substrates covered with graphene has been proposed (Fig. 5f). Weak interactions allow lattice-matched epitaxy together with easier mechanical release[93] and heteroepitaxy with a spontaneous relaxation of misfit strain[94]. The technique has been applied to transferred LEDS[93], but not to photovoltaics yet. Large surface area and defect-free epitaxial growth still seems limited by the localized defects in the transferred graphene.

**Ultrathin CIGS solar cells.** The fabrication of polycrystalline CIGS ultrathin layers on back reflectors raises specific challenges. CIGS are usually grown by co-evaporation, sputtering or electrodeposition on Mo, a refractory material that forms an ohmic contact with the CIGS thanks to the creation of a thin $MoSe_2$ interface layer.

Alternative back contact materials with higher optical reflectance and lower surface recombination are currently under investigation in several groups[66,67,70]. Silver mirrors encapsulated with transparent conducting oxides appear as a promising candidate[68].

## Light-trapping nanostructures for ultrathin devices

A key challenge for ultrathin solar cells is to enhance the light path in the cell to maintain a high absorption despite the thickness reduction. As discussed previously, submicrometre patterning is needed to scatter light or create multiple resonances in the absorber. Photolithography technologies using a projection lithography stepper[21], interferences[95] or the Talbot effect[96,97] are contactless techniques that meet the requirements for spatial resolution. However, their cost and long exposure time limit their use to proof-of-concept devices on small areas. In the framework of solar cell fabrication, specific techniques are required to structure matter at the nanoscale while being low-cost, scalable (patterned area >15 x 15 $cm^2$) and versatile (in particular compatible to non-planar substrates). Figure 6 gathers nanopatterning techniques that we envision as promising for structuring ultrathin solar cells.

The use of the ordered (Fig. 6a–c) or disordered (Fig. 6d–f) self-assembly of colloidal particles (usually made of silica or polystyrene) is a simple patterning technique called nanosphere lithography. Close-packed arrangements are obtained by self-assembly of particles at the air/water interface due to capillary forces (Fig. 6a–c). The colloidal crystal obtained can then be used as a mask or directly integrated in the solar cell as a diffractive structure (Fig. 6c)[63,98]. The scalability of close-packed colloidal assembly has been demonstrated over 1 $m^2$ glass substrates[99]. An alternative technique, sparse assembly, relies on electrostatic forces as particle–particle repulsion and particle–substrate attraction. It leads to an amorphous-ordered arrangement (Fig. 6e–f), which increases the number of accessible optical modes and can be of interest to achieve omnidirectional absorption. Sparse assembly has been used to texture the solar cell absorber[100,101] or to integrate plasmonic antennas[102]. This technique combined with dry etching was employed to structure a 1.1-µm-thick c-Si layer with parabolic holes (Fig. 6f)[23].

Nanoimprint lithography and its variants (Fig. 6g–i) offer more flexibility in the design of patterns, from periodic arrays of squares[103] or pyramids[22] to disordered structures[104,105]. This replication technique is based on the embossing of a polymeric resist or a sol-gel derived metal-oxide material with a hard mould containing nanoscale surface-relief features[106]. To reduce costs, soft NIL uses a single expensive master mould replicated into many cheap polymeric stamps[107]. Their flexibility allows low pressure embossing with a high tolerance to the substrate topography (Fig. 6g). It can be used as a conventional lithography technique with an additional step of pattern transfer. Using a Cr mask made by soft NIL, an inverted pyramid array was etched in a 3-µm-thick silicon solar cell (Fig. 6h–i)[22]. Alternatively, the replicated nanostructures can be directly integrated without additional pattern transfer[45,108], as demonstrated at the back contact of a III–V on Si triple junction solar cell using a roll-to-plate nanoimprint of SU8 resist (Fig. 6k–l)[103]. It should be noted that current automated systems can pattern substrates as large as 0.5 x 0.5 $m^2$ with resolution down to 20 nm and at high throughput[109].

## Collecting charge carriers

On both sides of the absorber, additional layers are needed to passivate the surfaces and collect charge carriers selectively at the contacts. Under illumination, photogenerated carriers thermalize at the band edges and are described by two quasi-Fermi distributions. The collection of carriers should occur before recombination to ensure a high $J_{sc}$, and the quasi-Fermi level splitting should be maintained through the selective contacts to maximize the $V_{oc}$.

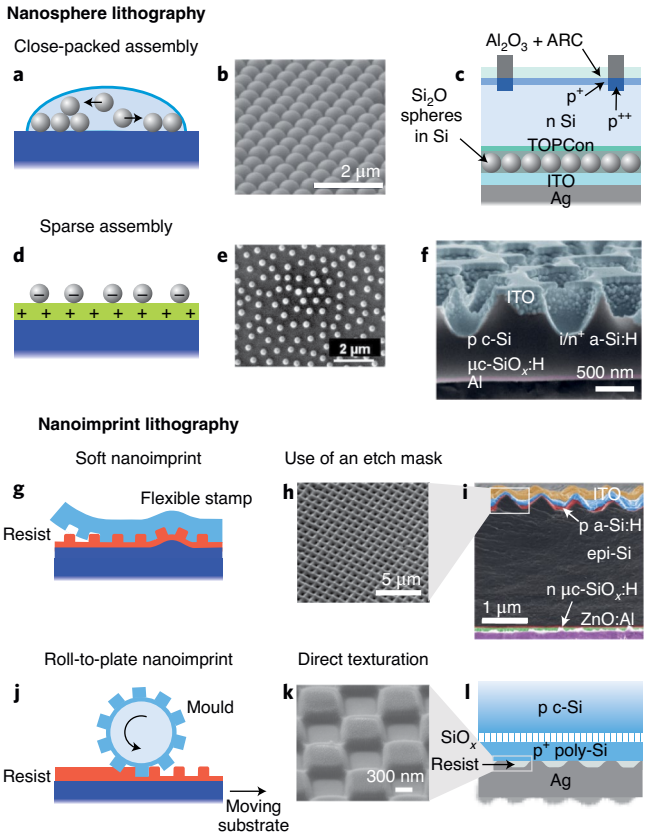


**Fig. 6 | Techniques to fabricate nanostructures and examples of integration in solar cells. a–f**, Nanosphere lithography: schematics of air–water colloidal assembly (**a**); SEM image of a close-packed assembly of 700-nm-large polystyrene nanospheres[99] (**b**); schematics of a silicon solar cell integrating silica nanospheres at the rear between a tunnel oxide passivated contact (TOPCon) layer and an indium tin oxide (ITO) spacer[98] (**c**); schematics of a sparse colloidal assembly relying on electrostatic interactions between charged colloids deposited on an oppositely charged substrate (**d**); SEM image of the resulting amorphous colloidal distribution (sphere size, 270 nm)[101] (**e**); SEM side view of an ultrathin (1.1 µm) silicon solar cell nanotextured using sparse colloidal assembly[23] (**f**). µc, microcrystalline. **g–l**, Nanoimprint lithography: schematics of the soft nanoimprint technique (**g**); SEM top view and cross-section of an ultrathin silicon solar cell textured with inverted pyramids using a nanoimprinted etch mask[22] (**h**,**i**); schematics of the roll-to-plate nanoimprint technique (**j**); SEM image of a SU8 resist grating made by roll-to-plate nanoimprint (**k**) and schematics of a silicon solar cell integrating the nanoimprinted SU8 grating in the back contact[103] (**l**). Panels reproduced with permission from ref. [99], American Chemical Society (**b**); ref. [101], The Optical Society (**e**); ref. [23], IOP (**f**); and ref. [103], Springer Nature Ltd (**k**). Panels adapted with permission from ref. [98], Elsevier (**c**); ref. [22], American Chemical Society (**h**,**i**); and ref. [103], Springer Nature Ltd. (**l**).

**Passivation.** While defect-assisted (Shockley–Read–Hall) recombination decreases proportionally to the absorber thickness $t$, the relative impact of surface recombination increases with the surface to volume ratio as $1/t$. Recombinations at the surface are mediated by states with energies located in the forbidden bandgap, that originate from dangling bonds or defects at the interface between the absorber and a different material. Their density can be decreased by covering the absorber surface with dielectric layers ($SiO_2$ or a-Si:H on c-Si, or sulfur-based compounds on III–V). Alternatively, their impact can be reduced by 'field effect' passivation using charged dielectric layers ($Al_2O_3$ on Si), or composition gradients to repel

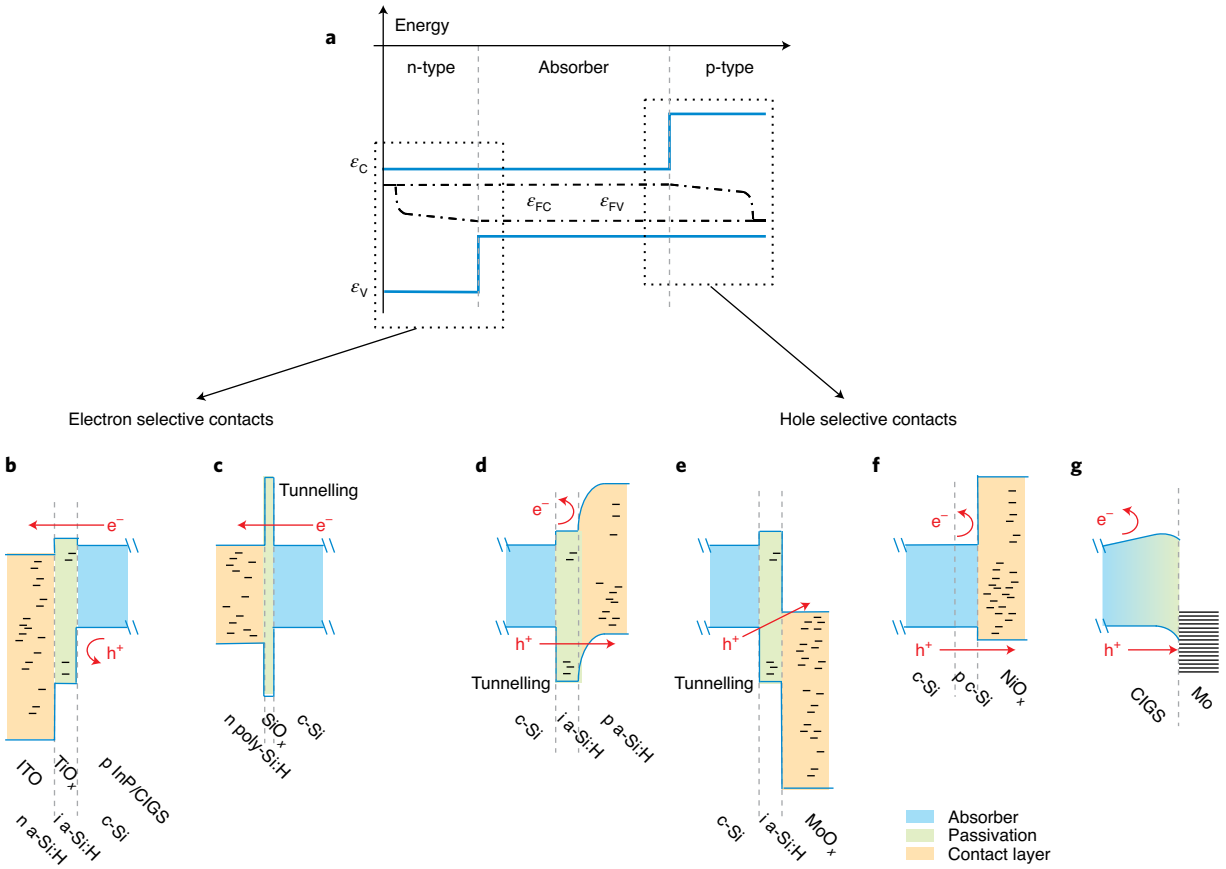


**Fig. 7 | Heterostructures for passivating selective contacts. a**, Band diagram of an ideal solar cell using n-type and p-type heterocontacts. The conduction and valence bands are indicated as $\varepsilon_C$ and $\varepsilon_V$ respectively (solid blue lines). The electron and hole quasi-Fermi levels, $\varepsilon_{FC}$ and $\varepsilon_{FV}$ respectively, are indicated with dash-dotted lines. **b**–**g**, Schematic band diagrams for illuminated solar cells at the maximum power point. The contacts are made of a first passivation layer (green), which decreases the density of surface defects or repels minority charges, and a second layer (orange) with appropriate band offsets, which creates a selective contact for majority carriers. The dashed boxes point to examples of implementation of selective and passivating contacts for electrons (**b**,**c**) and holes (**d**–**g**). Defect states in the gap are sketched with (–) marks. Diagrams of intrinsic and n-type a-Si:H layers for passivation and electron contact used in record c-Si solar cells[6], and a similar $TiO_x$/ITO scheme[174] on InP[175] and CIGS[176] (**b**); tunnel oxide passivating contacts (TOPCon) on Si[177,178] implemented in 25.7% efficiency with full-area contacts[179] (**c**); intrinsic and p-type a-Si:H layers for passivation and hole contacts (**d**); hole contact made of large work function n-type MoO*x*, using hole tunnelling through an intrinsic a-Si:H passivation layer on Si[180–182](**e**); $NiO_x$ p-type TCO used in combination with a p-type polycrystalline Si layer[150] (**f**); and CIGS/Mo contact showing a gradient of the indium to gallium ratio that leads to a shift of the conduction band maximum and contributes to the passivation of the ohmic hole contact[183,184] (**g**).

minority carriers from the defective interface in CIGS. To combine passivation and collection of carriers, insulating passivation layers with local doping or metallic point contacts have been the most developed workaround in conventional crystalline silicon solar cells since the 90s[110] and more recently in CIGS[60].

**Selective contacts by doping.** The separation of carriers occurs thanks to the different conductivities of electrons and holes[111], obtained by doping in homojunctions. However, ultrathin absorbers require relatively high doping: first, to keep the space charge layer confined in the junction thickness and ensure maximal $V_{OC}$ (>$10^{18}$ cm$^{-3}$ is required for 60-nm-thick GaAs) and, second, to preserve the selectivity of the contacts under illumination (the conductivity of minority carriers increases with the density of photogenerated charge carriers as $1/t$, assuming constant absorption). Heavy doping may induce many detrimental effects: increased long-wavelength parasitic absorption by free carriers, increased non-radiative recombination (defects, Auger), lower $V_{OC}$ due to bandgap narrowing (about 25 meV for $10^{18}$ cm$^{-3}$). Furthermore, high doping levels are not yet achievable for some materials such as CIGS and CdTe.

**Heterocontacts.** Heterostructures provide a way to overcome previous limitations and to design full-area passivating selective contacts. Wide bandgap materials with the appropriate band offset (Fig. 7a) can act as selective contacts forming a high energetic barrier to prevent minority carrier recombination while enabling favourable band alignment and being highly conductive for majority carriers. Due to their wide band-gap and low density of minority carriers even under illumination, the constraints on doping are relaxed. In the case of III–V materials, suitable alloys can be grown lattice-matched on GaAs[3]. For other technologies (c-Si, polycrystalline thin films), heterocontacts are made of dissimilar materials with lattice-mismatched or crystalline/amorphous interfaces, which are generally responsible for surface defects (Fig. 7). A stack of disordered materials is commonly used for both surface passivation and carrier selectivity with a suitable band offset or carrier tunnelling mechanism.

These solutions are usually integrated in planar solar cells, but most of these approaches can be implemented on textured absorbers using conformal deposition methods, opening new possibilities to combine heterostructures and light trapping in ultrathin solar

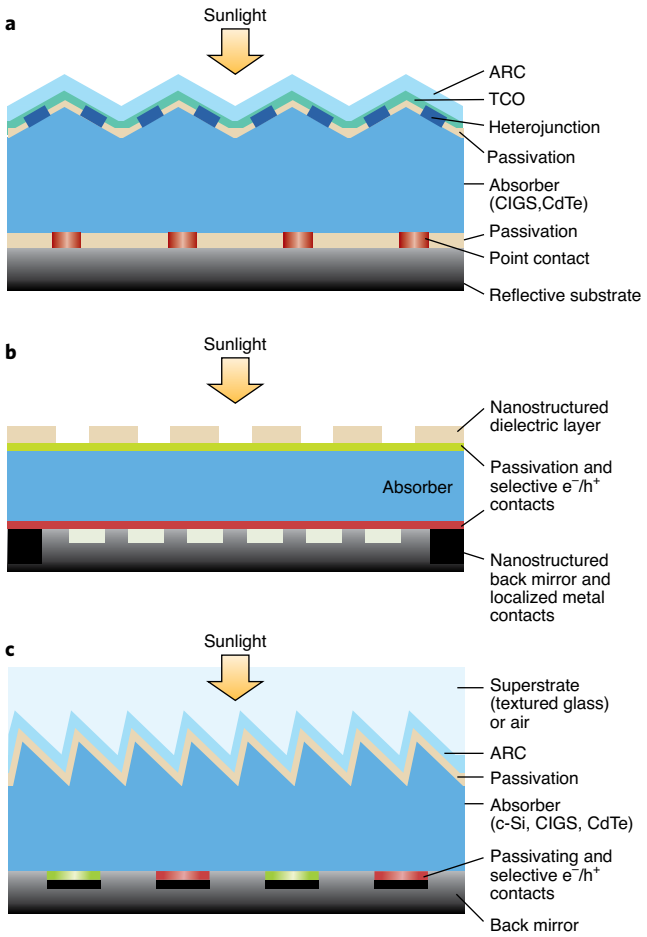


**Fig. 8 | Envisioned architectures for ultrathin solar cells.** These architectures integrate recent advances in light trapping, point contacts and heterostructures. **a**, Ultrathin CIGS solar cell with localized heterojunction and texturation at the front and point contacts on a back reflective substrate. **b**, Planar heterojunction solar cells that can be made of lattice-matched III–V semiconductors with front and back nanostructured layers and localized contacts. **c**, Asymmetric front texturation with complete passivation for optimal low-loss light trapping and interdigited back contacts embedded in a mirror. This design is derived from interdigited back contact c-Si solar cells and can be adapted to CIGS and CdTe photovoltaic devices in superstrate configuration.

cell designs. The solutions currently available should be further expanded by research on new materials and interfaces. For instance, wider bandgap semiconductors or TCO with an appropriate band offset could help lower parasitic absorption in the contact layers, in particular for hole collection.

## Novel architectures for ultrathin solar cells

In Fig. 8, we propose new architectures for ultrathin solar cells that integrate both photonic and electronic aspects, implementing strategies we foresee as most promising to bridge the gap between state-of-the-art and theoretical expectations.

In Fig. 8a, an ultrathin solar cell is designed with a front texturation for light trapping and localized selective contacts at both the front and back sides. This configuration ensures efficient carrier collection through point contacts while providing good passivation and optical transparency over most of the surface area. It also relieves the requirements on the contact materials. This architecture is particularly relevant for CIGS solar cells, with localized CdS/CIGS heterojunctions as a front contact[112,113], and Mo/CIGS ohmic point contacts combined with a reflective and conductive layer at the back side. Note that the back-point contacts can also be designed to contribute to light trapping through scattering or diffraction.

In Fig. 8b, the absorber is kept planar to lower surface recombination and selective electron–hole contact layers are implemented to provide efficient passivation. Light trapping is achieved with both front and back periodical nanopatterning, and a back mirror. The distance between localized ohmic contacts is defined according to the lateral conductivities in order to avoid series resistances. This architecture is currently achievable with III–V semiconductors[45] and could be applied to other technologies provided that transparent and passivating materials are available for the front and back selective contacts.

In Fig. 8c, interdigitated back contacts (IBC) are used for electron–hole selective collection of carriers. This design is an effective way to avoid parasitic absorption of high-energy photons in contact layers. It has already been successfully used in thick crystalline silicon solar cells, and could be adapted to polycrystalline CIGS[114] and CdTe thin films. This design could be fabricated by deposition on a textured and passivated glass substrate leading to a superstrate configuration. The contact spacing needs to be a few micrometres or less to match with the diffusion length of photogenerated carriers and the contact area should be minimized to keep a high overall reflectivity. In this example, optimal sunlight absorption is ensured by the combination of a back mirror and front patterning with submicrometre asymmetric periodical structures.

These examples show that recent advances in the design and fabrication of light-trapping structures and selective contacts can be combined into ultrathin solar cells, enabling high performance. Nevertheless, some practical challenges still need to be addressed. First, novel materials and processing techniques are necessary. For instance, in the architecture of Fig. 8b, absorption losses at short wavelengths should be further reduced in the front-passivating and selective contact layers. Furthermore, the materials used on the backside as the selective contact and mirror should sustain the high temperature required for the deposition of the absorber layers. For hole-selective contacts, p-type materials with a wide bandgap and a low electron affinity or hybrid solutions with tunnelling through an electron transport layer need to be developed. Second, there is an increasing need for patterning to improve cell performances. Multiscale patterning, such as structuring nanoholes on a microtextured surface, will bring an additional functionality to the front contact by combining localized contacts with micrometre scale light-trapping structures, as highlighted in Fig. 8a. As for the back contact, IBC thin film solar cells (Fig. 8c) require contact spacing and alignment at the micrometre scale, which is several orders of magnitude smaller than for current IBC silicon solar cells.

## Outlook

We believe that the advances in light trapping for ultrathin solar cells will also be beneficial to conventional (thicker) solar cells for further increase of $J_{sc}$, photon recycling and lower parasitic absorption losses. Photon management can also be used for thermal control of photovoltaic devices. The decrease of absorption in the sub-bandgap infrared region with optimized TCO and highly-reflective back mirrors limits overheating and increases energy production. Further optimization of the emissivity of solar cells in the far-infrared spectral range may even lead to passive radiative cooling under direct sunlight[115].

Low temperature fabrication of ultrathin semiconductor layers as well as layer transfer techniques can offer several key advantages for flexible and high power-to-weight ratio photovoltaic applications[116], for example, building-integrated photovoltaics or remote power applications such as electric vehicles and aircrafts. In the case of photovoltaics systems used in space, the impact of the absorber

degradation due to particle bombardment decreases dramatically in very thin layers[117].

Looking further ahead, enhanced absorption in ultrathin semiconductor volumes allows for operating the device at high photo-generated carrier densities, a physical regime required in advanced high-efficiency concepts such as hot-carrier solar cells or intermediate band solar cells[118,119]. Ultrathin multijunction solar cells may also be a promising application. Yet they will present new challenges of combining efficient light trapping on an overall broadband spectrum with current matching between the subcells[120].

In this Review, we have highlighted the dynamism of research on ultrathin solar cells based on c-Si, GaAs and CIGS materials and we have presented general concepts that could also foster advances in other technologies. Such fabrication and patterning concepts should be developed further to make them upscalable, cost effective and industrially viable.

Received: 11 July 2019; Accepted: 22 September 2020;
Published online: 2 November 2020

## References


1. Renewable power generation by technology in the Sustainable Development Scenario, 2000-2030. *IEA* https://www.iea.org/data-and- statistics/charts/renewable-power-generation- by-technology-in-the-sustainable-development- scenario-2000-2030 (2020).
2. Shockley, W. & Queisser, H. J. Detailed balance limit of efficiency of p-n junction solar cells. *J. Appl. Phys.* **32**, 510–519 (1961).
3. Kayes, B. M. et al. 27.6% conversion efficiency, a new record for single-junction solar cells under 1 sun illumination. In *Proc. 37th IEEE Photovoltaic Specialists Conference* 4–8 (2011).
4. Green, M. A. et al. Solar cell efficiency tables (version 53). *Prog. Photovolt.* **27**, 3–12 (2019).
5. Richter, A., Hermle, M. & Glunz, S. W. Reassessment of the limiting efficiency for crystalline silicon solar cells. *IEEE J. Photovolt.* **3**, 1184–1191 (2013).
6. Yoshikawa, K. et al. Silicon heterojunction solar cell with interdigitated back contacts for a photoconversion efficiency over 26%.*Nat. Energy* **2**, 17032 (2017).
**High-efficiency heterojunction solar cells with $e^-$ /$h^+$ selective contacts**.
7. Nakamura, M. et al. Cd-Free Cu(In, Ga)(Se, S)$_2$ thin-film solar cell with record efficiency of 23.35%. *IEEE J. Photovolt.* **9**, 1863–1867 (2019).
8. Andreani, L. C., Bozzola, A., Kowalczewski, P., Liscidini, M. & Redorici, L. Silicon solar cells: toward the efficiency limits. *Adv. Phys. X* **4**, 1548305 (2019).
9. Miller, O. D., Yablonovitch, E. & Kurtz, S. R. Strong internal and external luminescence as solar cells approach the Shockley–Queisser limit. *IEEE J. Photovolt.* **2**, 303–311 (2012).
10. Sai, H. et al. Potential of very thin and high-efficiency silicon heterojunction solar cells. *Prog. Photovolt.* **27**, 1061–1070 (2019).
11. Liu, Z. et al. Revisiting thin silicon for photovoltaics: a technoeconomic perspective. *Energy Environ. Sci.* **13**, 12–23 (2020).
12. Bhattacharya, S., Baydoun, I., Lin, M. & John, S. Towards 30% power conversion efficiency in thin-silicon photonic-crystal solar cells. *Phys. Rev. Appl.* **11**, 014005 (2019).
13. Petermann, J. H. et al. 19%-efficient and 43 µm-thick crystalline Si solar cell from layer transfer using porous silicon. *Prog. Photovolt.* **20**, 1–5 (2012).
**CVD epitaxial growth of c-Si layers ($t$ = 43 µm) on recrystallized porous silicon and transfer**.
14. Haug, F.-J. & Ballif, C. Light management in thin film silicon solar cells. *Energy Environ. Sci.* **8**, 824–837 (2015).
15. Erwin, W. R., Zarick, H. F., Talbert, E. M. & Bardhan, R. Light trapping in mesoporous solar cells with plasmonic nanostructures. *Energy Environ. Sci.* **9**, 1577–1601 (2016).
16. Liu, J., Yao, M. & Shen, L. Third generation photovoltaic cells based on photonic crystals. *J. Mater. Chem. C* **7**, 3121–3145 (2019).
17. Jena, A. K., Kulkarni, A. & Miyasaka, T. Halide perovskite photovoltaics: background, status, and future prospects. *Chem. Rev.* **119**, 3036–3103 (2019).
18. Powalla, M. et al. Thin-film solar cells exceeding 22 % solar cell efficiency: an overview on CdTe-, Cu(In, Ga)Se2-, and perovskite-based materials. *Appl. Phys. Rev.* **5**, 041602 (2018).
19. Liu, X. et al. The current status and future prospects of kesterite solar cells: a brief review. *Prog. Photovolt.* **24**, 879–898 (2016).
20. Wang, A., Zhao, J., Wenham, S. R. & Green, M. A. 21.5% Efficient thin silicon solar cell. *Prog. Photovolt.* **4**, 55–58 (1996).
21. Branham, M. S. et al. 15.7% Efficient 10-µm-thick crystalline silicon solar cells using periodic nanostructures. *Adv. Mater.* **27**, 2182–2188 (2015).
**This paper reports the first ultrathin silicon solar cell ($t$ = 10 µm) with a short-circuit current exceeding significantly single-pass absorption and leading to an efficiency $\eta$ = 15.7%.**
22. Gaucher, A. et al. Ultrathin epitaxial silicon solar cells with inverted nanopyramid arrays for efficient light trapping. *Nano Lett.* **16**, 5358–5364 (2016).
23. Depauw, V. et al. Sunlight-thin nanophotonic monocrystalline silicon solar cells. *Nano Futures* **1**, 021001 (2017).
24. Zhou, S. et al. Wafer-scale integration of inverted nanopyramid arrays for advanced light trapping in crystalline silicon thin film solar cells. *Nanoscale Res. Lett.* **11**, 194 (2016).
25. Kuang, P. et al. Achieving an accurate surface profile of a photonic crystal for near-unity solar absorption in a super thin-film architecture. *ACS Nano* **10**, 6116–6124 (2016).
26. Chong, T. K., Wilson, J., Mokkapati, S. & Catchpole, K. R. Optimal wavelength scale diffraction gratings for light trapping in solar cells. *J. Opt.* **14**, 024012 (2012).
27. Wang, K. X., Yu, Z., Liu, V., Cui, Y. & Fan, S. Absorption enhancement in ultrathin crystalline silicon solar cells with antireflection and light-trapping nanocone gratings. *Nano Lett.* **12**, 1616–1619 (2012).
28. Eyderman, S. et al. Light-trapping optimization in wet-etched silicon photonic crystal solar cells. *J. Appl. Phys.* **118**, 023103 (2015).
29. Eyderman, S., John, S. & Deinega, A. Solar light trapping in slanted conical-pore photonic crystals: beyond statistical ray trapping. *J. Appl. Phys.* **113**, 154315 (2013).
30. Martins, E. R. et al. Deterministic quasi-random nanostructures for photon control. *Nat. Commun.* **4**, 2665 (2013).
31. Meng, X. et al. Combined front and back diffraction gratings for broadband light trapping in thin film solar cells. *Opt. Express* **20**, A560–A571 (2012).
32. Shi, Y., Wang, X., Liu, W., Yang, T. & Yang, F. Light-absorption enhancement in thin-film silicon solar cells with front grating and rear-located nanoparticle grating. *Phys. Status Solidi.* **212**, 312–316 (2014).
33. Haug, F.-J., Söderström, T., Cubero, O., Terrazzoni-Daudrix, V. & Ballif, C. Influence of the ZnO buffer on the guided mode structure in Si/ZnO/Ag multilayers. *J. Appl. Phys.* **106**, 044502 (2009).
34. Lee, H.-S. et al. Enhanced efficiency of crystalline Si solar cells based on kerfless-thin wafers with nanohole arrays. *Sci. Rep.* **8**, 3504 (2018).
35. Ingenito, A., Isabella, O. & Zeman, M. Experimental demonstration of $4n^2$ classical absorption limit in nanotextured ultrathin solar cells with dielectric omnidirectional back reflector. *ACS Photonics* **1**, 270–278 (2014).
36. Zeng, L. et al. Demonstration of enhanced absorption in thin film Si solar cells with textured photonic crystal back reflector. *Appl. Phys. Lett.* **93**, 221105 (2008).
37. Green, M. A. & Ho-Baillie, A. W. Y. Pushing to the limit: radiative efficiencies of recent mainstream and emerging solar cells. *ACS Energy Lett.* **4**, 1639–1644 (2019).
38. Nakayama, K., Tanabe, K. & Atwater, H. A. Plasmonic nanoparticle enhanced light absorption in GaAs solar cells. *Appl. Phys. Lett.* **93**, 121904 (2008).
39. Liu, W. et al. Surface plasmon enhanced GaAs thin film solar cells. *Sol. Energy Mater. Sol. Cells* **95**, 693–698 (2011).
40. Yang, W. et al. Ultra-thin GaAs single-junction solar cells integrated with a reflective back scattering layer. *J. Appl. Phys.* **115**, 203105 (2014).
41. Vandamme, N. et al. Ultrathin GaAs solar cells with a silver back mirror. *IEEE J. Photovolt.* **5**, 565–570 (2015).
42. van Eerden, M. et al. A facile light-trapping approach for ultrathin GaAs solar cells using wet chemical etching. *Prog. Photovolt.* **28**, 200–209 (2020).
43. Grandidier, J., Callahan, D., Munday, J. & Atwater, H. A. Gallium arsenide solar cell absorption enhancement using whispering gallery modes of dielectric nanospheres. *IEEE J. Photovolt.* **2**, 123–128 (2012).
44. Lee, S.-M. et al. High performance ultrathin GaAs solar cells enabled with heterogeneously integrated dielectric periodic nanostructures. *ACS Nano* **9**, 10356–10365 (2015).
45. Chen, H.-L. et al. A 19.9%-efficient ultrathin GaAs solar cell with a silver nanostructured back mirror. *Nat. Ener.* **4**, 761–767 (2019).
**This paper reports the fabrication of an ultrathin GaAs solar cell ($t$ = 205 nm) with a nanostructured back mirror and a conversion efficiency close to 20%.**
46. Massiot, I. et al. Metal nanogrid for broadband multiresonant light-harvesting in ultrathin GaAs layers. *ACS Photonics* **1**, 878–884 (2014).
47. Eyderman, S., Deinega, A. & John, S. Near perfect solar absorption in ultra-thin-film GaAs photonic crystals. *J. Mater. Chem. A* **2**, 761–769 (2014).
48. Eyderman, S. & John, S. Light-trapping and recycling for extraordinary power conversion in ultra-thin gallium-arsenide solar cells. *Sci. Rep.* **6**, 28303 (2016).
49. Aberg, I. et al. A GaAs nanowire array solar cell with 15.3% efficiency at 1 sun. *IEEE J. Photovolt.* **6**, 185–190 (2016).
50. Horowitz, K. A. W., Fu, R. & Woodhouse, M. An analysis of glass-glass CIGS manufacturing costs. *Sol. Energy Mater. Sol. Cells* **154**, 1–10 (2016).

51. Shafarman, W. N. et al. Effect of reduced deposition temperature, time, and thickness on Cu(InGa)$Se_2$ films and devices. In *Proc. 26th IEEE Photovoltaic Specialists Conference* 331–334 (IEEE, 1997).
52. Lundberg, O., Bodegard, M., Malmström, J. & Stolt, L. Influence of the Cu(In, Ga)$Se_2$ thickness and Ga grading on solar cell performance. *Prog. Photovolt.* **11**, 77–88 (2003).
53. Jehl, Z. et al. Thinning of CIGS solar cells: Part II: cell characterizations. *Thin Solid Films* **519**, 7212–7215 (2011).
54. Han, A. et al. Structure, morphology and properties of thinned Cu(In, Ga)$Se_2$ films and solar cells. *Semicond. Sci. Technol.* **27**, 035022 (2012).
55. Reinhard, P. et al. Flexible Cu(In, Ga)$Se_2$ solar cells with reduced absorber thickness. *Prog. Photovolt.* **23**, 281–289 (2013).
56. Pettersson, J., Törndahl, T., Platzer-Björkman, C., Hultqvist, A. & Edoff, M. The influence of absorber thickness on Cu(In, Ga)$Se_2$ solar cells with different buffer layers. *IEEE J. Photovolt.* **3**, 1376–1382 (2013).
57. Leonard, E. et al. Cu(In, Ga)$Se_2$ absorber thinning and the homo-interface model: Influence of Mo back contact and 3-stage process on device characteristics. *J. Appl. Phys.* **116**, 074512 (2014).
58. Jarzembowski, E. et al. Optical and electrical characterization of Cu(In, Ga)$Se_2$ thin film solar cells with varied absorber layer thickness. *Thin Solid Films* **576**, 75–80 (2015).
59. Yin, G., Brackmann, V., Hoffmann, V. & Schmid, M. Enhanced performance of ultra-thin Cu(In, Ga)$Se_2$ solar cells deposited at low process temperature. *Sol. Energy Mater. Sol. Cells* **132**, 142–147 (2015).
60. Vermang, B. et al. Employing Si solar cell technology to increase efficiency of ultra-thin Cu(In, Ga)$Se_2$ solar cells. *Prog. Photovolt.* **22**, 1023–1029 (2014). **This work demonstrates an ultrathin CIGS solar cell ($t$ = 385 nm) with a passivated back surface and nanosized point contacts ($\eta$ = 13.5%).**
61. Vermang, B. et al. Introduction of Si PERC rear contacting design to boost efficiency of Cu(In, Ga)Se2 solar cells. *IEEE J. Photovolt.* **4**, 1644–1649 (2014).
62. van Lare, C., Yin, G., Polman, A. & Schmid, M. Light coupling and trapping in ultrathin Cu(In, Ga)$Se_2$ solar cells using dielectric scattering patterns. *ACS Nano* **9**, 9603–9613 (2015).
63. Yin, G., Manley, P. & Schmid, M. Light absorption enhancement for ultra-thin Cu($In_{1-x}Ga_x$)$Se_2$ solar cells using closely packed 2-D $SiO_2$ nanosphere arrays. *Sol. Energy Mater. Sol. Cells* **153**, 124–130 (2016).
64. Jarzembowski, E., Fuhrmann, B., Leipner, H., Fränzel, W. & Scheer, R. Ultrathin Cu(In, Ga)$Se_2$ solar cells with point-like back contact in experiment and simulation. *Thin Solid Films* **633**, 61–65 (2016).
65. Malmström, J., Schleussner, S. & Stolt, L. Enhanced back reflectance and quantum efficiency in Cu(In, Ga)$Se_2$ thin film solar cells with a ZrN back reflector. *Appl. Phys. Lett.* **85**, 2634–2636 (2004).
66. Ohm, W. et al. Bifacial Cu(In, Ga)$Se_2$ solar cells with submicron absorber thickness: back-contact passivation and light management. In *Proc. 42nd IEEE Photovoltaic Specialists Conference*. 1–5 (IEEE, 2015).
67. Mollica, F. et al. Light absorption enhancement in ultra-thin Cu(In, Ga)$Se_2$ solar cells by substituting the back-contact with a transparent conducting oxide based reflector. *Thin Solid Films* **633**, 202–207 (2016).
68. Gouillart, L. et al. Development of reflective back contacts for high-efficiency ultrathin Cu(In, Ga)$Se_2$ solar cells. *Thin Solid Films* **672**, 1–6 (2019).
69. Jehl, Z. et al. Towards ultrathin copper indium gallium diselenide solar cells: proof of concept study by chemical etching and gold back contact engineering. *Prog. Photovolt.* **20**, 582–587 (2012).
70. Larsen, J. K., Simchi, H., Xin, P., Kim, K. & Shafarman, W. N. Backwall superstrate configuration for ultrathin Cu(In, Ga)$Se_2$ solar cells. *Appl. Phys. Lett.* **104**, 033901 (2014).
71. Dahan, N. et al. Optical approaches to improve the photocurrent generation in Cu(In, Ga)$Se_2$ solar cells with absorber thicknesses down to 0.5 µm. *J. Appl. Phys.* **112**, 094902 (2012).
72. Onwudinanti, C. et al. Advanced light management based on periodic textures for Cu(In, Ga)$Se_2$ thin-film solar cells. *Opt. Express* **24**, A693–A707 (2016).
73. Goffard, J. et al. Light trapping in ultrathin CIGS solar cells with nanostructured back mirrors. *IEEE J. Photovolt.* **7**, 1433–1441 (2017).
74. Bedell, S. W. et al. Kerf-less removal of Si, Ge, and III–V layers by controlled spalling to enable low-cost PV technologies. *IEEE J. Photovolt.* **2**, 141–147 (2012).
75. Saha, S. et al. Single heterojunction solar cells on exfoliated flexible ~25µm thick mono-crystalline silicon substrates. *Appl. Phys. Lett.* **102**, 163904 (2013). **Ultrathin silicon solar cell ($t$ = 25 µm) fabricated by exfoliation, a kerf-less process.**
76. Crouse, D. et al. Increased fracture depth range in controlled spalling of (100)-oriented germanium via electroplating. *Thin Solid Films* **649**, 154–159 (2018).
77. Sweet, C. A. et al. Controlled exfoliation of (100) GaAs-based devices by spalling fracture. *Appl. Phys. Lett.* **108**, 011906 (2016).
78. Bruel, M. Process for the production of thin semiconductor material films. US patent 5374564 (1994).
79. Mizushima, I., Sato, T., Taniguchi, S. & Tsunashima, Y. Empty-space-in-silicon technique for fabricating a silicon-on-nothing structure. *Appl. Phys. Lett.* **77**, 3290–3292 (2000).
80. Kapur, P. et al. A manufacturable, non-plated, non-Ag metallization based 20.44 % efficient, 243 $cm^2$ area, back contacted solar cell on 40 µm thick mono-crystalline silicon. In *Proc. 28th European Photovoltaic Solar Energy Conference and Exhibition* 2228–2231 (2013).
81. Wang, L. et al. Development of a 16.8% efficient 18-µm silicon solar cell on steel. *IEEE J. Photovolt.* **4**, 1397 (2014).
82. Cariou, R. et al. Ultra-thin PECVD epitaxial Si solar cells on glass via low temperature transfer process. *Prog. Photovolt.* **24**, 1075–1084 (2016).
83. Branz, H. M. et al. Hot-wire chemical vapor deposition of epitaxial film crystal silicon for photovoltaics. *Thin Solid Films* **519**, 4545–4550 (2011).
84. Brendel, R. et al. Monocrystalline Si waffles for thin solar cells fabricated by the novel-perforated silicon process. *Appl. Phys. A* **67**, 151 (1998).
85. Sakaguchi, K. et al. Current progress in epitaxial layer transfer. *IEICE Trans. Electron.* **378**, E80-C (1997).
86. Tayanaka, H., Yamauchi, K. & Matsuhita, T. Thin-film crystalline silicon solar cells obtained by separation of a porous silicon sacrificial layer. In *Proc. 2nd World Conference on Photovoltaic Energy Conversion* 1272 (1998).
87. Moslehi M. M. et al. World-record 20.6% efficiency 156 mm x 156 mm full-square solar cells using low-cost kerfless ultrathin epitaxial silicon & porous silicon lift-off technology for industry-leading high-performance smart PV modules. In *Proc. The PV Asia Pacific Conference* (2012).
88. Stern, F. & Woodall, J. M. Photon recycling in semiconductor lasers. *J. Appl. Phys.* **45**, 3904 (1974).
89. Konagai, M., Sugimoto, M. & Takahashi, K. High efficiency GaAs thin film solar cells by peeled film technology. *J. Cryst. Growth* **45**, 277–280 (1978).
90. Park, S. et al. Germanium-on-nothing for epitaxial liftoff of GaAs solar cells. *Joule* **3**, 1782–1793 (2019).
91. McClelland, R. W., Bolzer, C. O. & Fan, J. C. C. A technique for producing epitaxial films on reuseable substrates. *Appl. Phys. Lett.* **37**, 560 (1980).
92. Bozler, C. O., McClelland, R. W. & Fan, J. C. C. Ultrathin, high-efficiency solar cells made from GaAs films prepared by the CLEFT Process. *IEEE Electron Device Lett.* **2**, 203 (1981).
93. Kim, Y. et al. Remote epitaxy through graphene enables two-dimensional material-based layer transfer. *Nature* **544**, 340–343 (2017). **Epitaxial growth of III–V through graphene for easy layer transfer and substrate reuse.**
94. Bae, S. H. et al. Graphene-assisted spontaneous relaxation towards dislocation-free heteroepitaxy. *Nat. Nanotechnol.* **15**, 272–276 (2020).
95. Wolf, A. J. et al. Origination of nano- and microstructures on large areas by interference lithography. *Microelectron. Eng.* **98**, 293–296 (2012).
96. Solak, H., Dais, C. & Clube, F. Displacement Talbot lithography: a new method for high-resolution patterning of large areas. *Opt. Express* **19**, 10686 (2011).
97. Wang, L. et al. Sub-wavelength printing in the deep ultra-violet region using Displacement Talbot Lithography. *Microelectron. Eng.* **161**, 104–108 (2016).
98. Eisenlohr, J. et al. Rear side sphere gratings for improved light trapping in crystalline silicon single junction and silicon-based tandem solar cells. *Sol. Energy Mater. Sol. Cells* **142**, 60–65 (2015).
99. Gao, P. et al. Large-area nanosphere self-assembly by a micro-propulsive injection method for high throughput periodic surface nanotexturing. *Nano Lett.* **15**, 4591–4598 (2015).
100. Massiot, I. et al. Highly conformal fabrication of nanopatterns on non-planar surfaces. *Nanoscale* **8**, 11461 (2016).
101. Trompoukis, C. et al. Disordered nanostructures by hole-mask colloidal lithography for advanced light-trapping in silicon solar cells. *Opt. Express* **24**, A191–201 (2016).
102. El Daif, O. et al. Front side plasmonic effect on thin silicon epitaxial solar cells. *Sol. Energy Mater. Sol. Cells* **104**, 58–63 (2012).
103. Cariou, R. et al. III-V-on-silicon solar cells reaching 33 % photoconversion efficiency in two-terminal configuration. *Nat. Ener.* **3**, 326–333 (2018).
104. Battaglia, C. et al. Nanoimprint lithography for high-efficiency thin-film silicon solar cells. *Nano Lett.* **11**, 661–665 (2011).
105. Battaglia, C. et al. Nanomoulding of transparent zinc oxide electrodes for efficient light trapping in solar cells. *Nat. Photon.* **5**, 535–538 (2011).
106. Chou, S. Y., Krauss, P. R. & Renstrom, P. J. Imprint of sub-25 nm vias and trenches in polymers. *Appl. Phys. Lett.* **67**, 3114 (1995).
107. Odom, T. W. et al. Improved pattern transfer in soft lithography using composite stamps. *Langmuir* **18**, 5314 (2002).
108. Yin, G. et al. Optoelectronic enhancement of ultrathin CIGS solar cells by nanophotonic contacts. *Adv. Opt. Mater.* **5**, 1600637 (2017).
109. Lan H. *Large-Area Nanoimprint Lithography and Applications* (Intechopen, 2017).
110. Battaglia, C., Cuevas, A. & De Wolf, S. High-efficiency crystalline silicon solar cells: status and perspectives. *Energy Environ. Sci.* **9**, 1552–1576 (2016).

111. Würfel, U., Cuevas, A. & Würfel, P. Charge carrier separation in solar cells. *IEEE J. Photovolt.* **5**, 461–469 (2015).
**Different conductivities for $e^-/h^+$ is the key ingredient for charge carrier separation in solar cells. Heterojunctions might also provide passivation.**
112. Fu, Y. et al. ZnS nanodot film as defect passivation layer for Cu(In, Ga)$(S, Se)_2$ thin-film solar cells deposited by spray-ILGAR (Ion-Layer Gas Reaction). *Adv. Ener. Mater.* **1**, 561–564 (2011).
113. Reinhard, P. et al. Alkali-templated surface nanopatterning of chalcogenide thin films: a novel approach toward solar cells with enhanced efficiency. *Nano Lett.* **15**, 3334–3340 (2015).
**Introduction of local heterojunctions in passivated front surfaces of CIGS solar cells. Surface nanopatterning based on self-assembled and well-defined alkali condensate nanostructures.**
114. Rezaei, N., Isabella, O., Procel, P., Vroon, Z. & Zeman, M. Optical study of back-contacted CIGS solar cells. *Opt. Express* **27**, A269–A279 (2019).
115. Fan, S. Thermal photonics and energy applications. *Joule* **1**, 264–273 (2017).
116. Reese, M. O. et al. Increasing markets and decreasing package weight for high-specific-power photovoltaics. *Nat. Ener.* **3**, 1002–1012 (2018).
117. Hirst, L. C. et al. Intrinsic radiation tolerance of ultra-thin GaAs solar cells. *Appl. Phys. Lett.* **109**, 033908 (2016).
118. Green, M. A. & Bremner, S. P. Energy conversion approaches and materials for high-efficiency photovoltaics. *Nat. Mater.* **16**, 23–34 (2017).
119. Okada, Y. et al. Intermediate band solar cells: recent progress and future directions. *Appl. Phys. Rev.* **2**, 021302 (2015).
120. Mellor, A., Hylton, N., Maier, S. & Ekins-Daukes, N. Interstitial light-trapping design for multi-junction solar cells. *Sol. Energy Mater. Sol. Cells* **159**, 212–218 (2017).
121. Do, K. S. et al. Experimental and simulation study for ultrathin (~100 μm) mono crystalline silicon solar cell with 156×156 $mm^2$ area. *Met. Mater. Int.* **20**, 545 (2014).
122. Taguchi, M. et al. 24.7 % record efficiency HIT solar cell on thin silicon wafer. *IEEE J. Photovolt.* **4**, 96–99 (2014).
123. Radhakrishna, H. S. et al. Heterojunction IBC solar cells on thin (< 50μm) epitaxial Si foils produced from kerfless layer transfer process. In *Proc. 33rd European Photovoltaic Solar Energy Conference and Exhibition* 740–744 (2017).
124. Danel, A. et al. Silicon heterojunction solar cells with open-circuit-voltage above 750mV. In *Proc. 35th European Photovoltaic Solar Energy Conference and Exhibition* 444–447 (2018).
125. Reuter, M., Brendle, W., Tobail, O. & Werner, J. H. 50 μm thin solar cells with 17.0% efficiency. *Sol. Energy Mater. Sol. Cells* **93**, 704–706 (2009).
126. Bergmann, R., Berge, C., Rinke, T., Schmidt, J. & Werner, J. Advances in monocrystalline Si thin film solar cells by layer transfer. *Sol. Energy Mater. Sol. Cells* **74**, 213–218 (2002).
127. Tang, Q. et al. Superiority of random inverted nanopyramid as efficient light trapping structure in ultrathin flexible c-Si solar cell. *Renew. Ener.* **133**, 883–892 (2019).
128. Balaji, P., Dauksher, W. J., Bowden, S. G., Augusto, A. Flexible silicon heterojunction solar cells on 40 μm thin substrates. In *Proc. IEEE 46th Photovoltaic Specialists Conference (PVSC)* 1089–1092 (IEEE, 2019).
129. Glunz, S. New concepts for high-efficiency silicon solar cells. *Sol. Energy Mater. Sol. Cells* **90**, 3276–3284 (2006).
130. Li, Y. et al. Quasi-Omnidirectional Ultrathin Silicon Solar Cells Realized by Industrially Compatible Processes. *Adv. Electron. Mater.* **5**, 1800858 (2019).
131. Zheng, G. et al. 16.4% efficient, thin active layer silicon solar cell grown by liquid phase epitaxy. *Sol. Energy Mater. Sol. Cells* **40**, 231–238 (1996).
132. Kuzma-Filipek, I. et al. 16% thin-film epitaxial silicon solar cells on 70-$cm^2$ area with 30-μm active layer, porous silicon back reflector, and Cu-based top-contact metallization. *P. rog. Photovolt.* **20**, 350–355 (2012).
133. Haase, F., Horbelt, R., Terheiden, B., Plagwitz, H. & Brendel, R. Back contact monocrystalline thin-film silicon solar cells from the porous silicon process. In *Proc. The 34th IEEE Photovoltaic Specialists Conference* 244–246 (2009).
134. Blakers, A. W. 17% Efficient thin-film silicon solar cell by liquid-phase epitaxy. *Prog. Photovolt.* **3**, 193–195 (1995).
135. Kim, H. J., Depauw, V., Duerinckx, F., Beaucarne, G. & Poortmans, J. Large-area thin-film free-standing monocrystalline Si solar cells by layer transfer. In *Proc. The IEEE 4th World Conference on Photovoltaic Energy Conference* 984–987 (IEEE, 2006).
136. Hilali, M. M. et al. Light trapping in ultrathin 25 μm exfoliated Si solar cells. *Appl. Opt.* **53**, 6140–6147 (2014).
137. He, J. et al. 15% Efficiency ultrathin silicon solar cells with fluorine-doped titanium oxide and chemically tailored poly(3,4-ethylenedioxythiophene): poly(styrenesulfonate) as asymmetric heterocontact. *ACS Nano* **13**, 6356–6362 (2019).
138. Wolf, A., Terheiden, B. & Brendel, R. Autodiffusion: a novel method for emitter formation in crystalline silicon thin-film solar cells. *Prog. Photovolt.* **15**, 199–210 (2007).
139. Duerinckx, F., Kuzma-Filipek, I., Nieuwenhuysen, K. V., Beaucarne, G. & Poortmans, J. Simulation and implementation of a porous silicon reflector for epitaxial silicon solar cells. *Prog. Photovolt.* **16**, 399–407 (2008).
140. Nieuwenhuysen, K. V. et al. Epitaxially grown emitters for thin film silicon solar cells result in 16% efficiency. *Thin Solid Films* **518**, S80–S82 (2010).
141. He, J. et al. Realization of 13.6% efficiency on 20 μm thick si/organic hybrid heterojunction solar cells via advanced nanotexturing and surface recombination suppression. *ACS Nano* **9**, 6522–6531 (2015).
142. Zheng, S., Wenham, R. & Green, M. A. 17.6% efficient multilayer thin-film silicon solar cells deposited on heavily doped silicon substrates. *Prog. Photovolt.* **4**, 369–373 (1996).
143. Jeong, S., McGehee, M. D. & Cui, Y. All-back-contact ultra-thin silicon nanocone solar cells with 13.7% power conversion efficiency. *Nat. Commun.* **4**, 2950 (2013).
144. Hadibrata, W., Es, F., Yerci, S. & Turan, R. Ultrathin Si solar cell with nanostructured light trapping by metal assisted etching. *Sol. Energy Mater. Sol. Cells* **180**, 247–252 (2018).
145. Wang, S. et al. Large-area free-standing ultrathin single-crystal silicon as processable materials. *Nano Lett.* **13**, 4393–4398 (2013).
146. Cariou, R., Ruggeri, R., Chatterjee, P., Gentner, J. L. & Roca I Cabarrocas, P. Silicon epitaxy below 200 °C: towards thin crystalline solar cells. In *Proc. SPIE Optics and Photonics* 84700B (SPIE, 2012).
147. Xue, M. et al. Free-standing 2.7 μm thick ultrathin crystalline silicon solar cell with efficiency above 12.0%. *Nano Ener.* **70**, 104466 (2020).
148. Cariou, R., Labrune, M. & Roca i Cabarrocas, P. Thin crystalline silicon solar cells based on epitaxial films grown at 165°C by RF-PECVD. *Sol. Energy Mater. Sol. Cells* **95**, 2260–2263 (2011).
149. Teplin, C. W. et al. Comparison of thin epitaxial film silicon photovoltaics fabricated on monocrystalline and polycrystalline seed layers on glass. *Prog. Photovolt.* **23**, 909–917 (2015).
150. Xue, M. et al. Contact selectivity engineering in a 2 μm thick ultrathin c-Si solar cell using transition-metal oxides achieving an efficiency of 10.8 %. *ACS Appl. Mater. Interfaces* **9**, 41863–41870 (2017).
151. Trompoukis, C., El Daif, O., Depauw, V., Gordon, I. & Poortmans, J. Photonic assisted light trapping integrated in ultrathin crystalline silicon solar cells by nanoimprint lithography. *Appl. Phys. Lett.* **101**, 103901 (2012).
152. Depauw, V., Qiu, Y., Van Nieuwenhuysen, K., Gordon, I. & Poortmans, J. Epitaxy-free monocrystalline silicon thin film: first steps beyond proof-of-concept solar cells. *Prog. Photovolt.* **19**, 844 (2011).
153. Mavrokefalos, A., Han, S. E., Yerci, S., Branham, M. S. & Chen, G. Efficient light trapping in inverted nanopyramid thin crystalline silicon membranes for solar cell applications. *Nano Lett.* **12**, 2792–2796 (2012).
154. Kuang, P. et al. Achieving an accurate surface profile of a photonic crystal for near-unity solar absorption in a super thin-film architecture. *ACS Nano* **10**, 6116–6124 (2016).
155. Hsu, W.-C. et al. Mismatched front and back gratings for optimum light trapping in ultra-thin crystalline silicon solar cells. *Opt. Commun.* **377**, 52–58 (2016).
156. Tan, X. et al. Enhancement of light trapping for ultrathin crystalline silicon solar cells. *Opt. Commun.* **426**, 584–588 (2018).
157. Kim, I. et al. Silicon nanodisk array design for effective light trapping in ultrathin c-Si. *Opt. Express* **22**, A1431–A1439 (2014).
158. Mallick, S. B., Agrawal, M. & Peumans, P. Optimal light trapping in ultra-thin photonic crystal crystalline silicon solar cells. *Opt. Express* **18**, 5691–5706 (2010).
159. Steiner, M. A. et al. Optical enhancement of the open-circuit voltage in high quality GaAs solar cells. *J. Appl. Phys.* **113**, 123109 (2013).
160. Gai, B. et al. Multilayer-grown ultrathin nanostructured GaAs solar cells as a cost-competitive materials platform for III–V photovoltaics. *ACS Nano* **11**, 992–999 (2017).
161. Yang, W. et al. Ultra-thin GaAs single-junction solar cells integrated with lattice-matched ZnSe as a reflective back scattering layer. In *Proc. 38th IEEE Photovoltaic Specialists Conference* 978–981 (IEEE, 2012).
162. Vandamme, N. *Nanostructured Ultrathin GaAs Solar Cells*. PhD thesis, Université Paris Sud (2015); http://www.theses.fr/2015PA112111.
163. Sai, H., Mizuno, H., Makita, K. & Matsubara, K. Light absorption enhancement in thin-film GaAs solar cells with flattened light scattering substrates. *J. Appl. Phys.* **122**, 123103 (2017).
164. Buencuerpo, J., Steiner, M. A. & Tamboli, A. C. Optically-thick 300 nm GaAs solar cells using adjacent photonic crystals. *Opt. Express* **28**, 13845 (2020).
165. Grenet, L. et al. Influence of coevaporation process on CIGS solar cells with reduced absorber thickness and current enhancement with periodically textured glass substrates. *Thin Solid Films* **621**, 188–194 (2017).
166. Kim, K., Park, H., Kim, W. K., Hanket, G. M. & Shafarman, W. N. Effect of reduced Cu(InGa)$(SeS)_2$ thickness using three-step $H_2Se/Ar/H_2S$ reaction of Cu-In-Ga metal precursor. *IEEE J. Photovolt.* **3**, 446–450 (2013).
167. Mansfield, L. M. et al. Efficiency increased to 15.2% for ultra-thin Cu(In, Ga)Se2 solar cells. *Prog. Photovolt.* **26**, 949–954 (2018).
168. Salome, P. M. P. et al. Passivation of interfaces in thin film solar cells: understanding the effects of a nanostructured rear point contact layer. *Adv. Mater. Interfaces* **5**, 1701101 (2018).

169. Shin, M. J. et al. Semi-transparent photovoltaics using ultra-thin Cu(In, Ga) $Se_2$ absorber layers prepared by single-stage co-evaporation. *Solar Ener.* **181**, 276–284 (2019).
170. Kim, K. & Shafarman, W. N. Alternative device structures for CIGS-based solar cells with semi-transparent absorbers. *Nano Ener.* **30**, 488–493 (2016).
171. Dahan, N. et al. Using radiative transfer equation to model absorption by thin Cu(In, Ga)$Se_2$ solar cells with Lambertian back reflector. *Opt. Express* **21**, 2563–2580 (2013).
172. Yin, G., Manley, P. & Schmid, M. Light trapping in ultrathin $CuIn_{1-x}Ga_xSe_2$ solar cells by dielectric nanoparticles. *Solar Ener.* **163**, 443–452 (2018).
173. Sasihithlu, K., Dahan, N. & Greffet, J. J. Light trapping in ultrathin CIGS solar cell with absorber thickness of 0.1 μm. *IEEE J. Photovolt.* **8**, 621–625 (2018).
174. Allen, T. G. et al. A low resistance calcium/reduced titania passivated contact for high efficiency crystalline silicon solar cells. *Adv. Ener. Mater.* **7**, 1602606 (2017).
175. Yin, X. et al. 19.2% Efficient InP heterojunction solar cell with electron-selective TiO2 contact. *ACS Photo.* **1**, 1245 (2014).
176. Hsu, W. et al. Electron-selective TiO2 contact for Cu(In, Ga)$Se_2$ solar cells. *Sci. Rep.* **5**, 16028 (2015).
177. Yablonovitch, E., Gmitter, T., Swanson, R. M. & Kwark, Y. H. A 720 mV open circuit voltage $SiO_x$:c-Si:$SiO_x$ double heterostructure solar cell. *Appl. Phys. Lett.* **47**, 1211–1213 (1985).
178. Feldmann, F. et al. Efficient carrier-selective p- and n-contacts for Si solar cells. *Sol. Energy Mater. Sol. Cells* **131**, 100–104 (2014).
179. Richter, A. et al. n-Type Si solar cells with passivating electron contact: identifying sources for efficiency limitations by wafer thickness and resistivity variation. *Sol. Energy Mater. Sol. Cells* **173**, 96–105 (2017).
180. Battaglia, C. et al. Hole selective $MoO_x$ contact for silicon solar cells. *Nano Lett.* **14**, 967–971 (2014).
181. Geissbühler, J. et al. 22.5 % efficient silicon heterojunction solar cell with molybdenum oxide hole collector. *Appl. Phys. Lett.* **107**, 081601 (2015).
182. Bullock, J. et al. Efficient silicon solar cells with dopant-free asymmetric heterocontacts. *Nat. Ener.* **1**, 15031 (2016).
183. Wei, S. & Zunger, A. Band offsets and optical bowings of chalcopyrites and Zn-based II-VI alloys. *J. Appl. Phys.* **78**, 3846–3856 (1995).
184. Feurer, T. et al. Progress in thin film CIGS photovoltaics – research and development, manufacturing, and applications. *Prog. Photovolt.* **7**, 645–667 (2016).
185. Green, M. A. & Keevers, M. J. Optical properties of intrinsic silicon at 300K. *Prog. Photovolt.* **3**, 189–192 (1995).
186. Yablonovitch, E. Statistical ray optics. *J. Opt. Soc. Am.* **71**, 899–907 (1982).
187. Green, M. A. Lambertian light trapping in textured solar cells and light-emitting diodes: analytical solutions. *Prog. Photovolt.* **10**, 235–241 (2002).
188. Collin, S. & Giteau, M. New limits for light-trapping with multi-resonant absorption. In *Proc. IEEE 7th World Conference on Photovoltaic Energy Conversion (WCPEC-7)* 3460–3462 (IEEE, 2018).
189. Wang, K. X., Guo, Y. & Fan, S. Wave optics light-trapping theory: mathematical justification and ultimate limit on enhancement. *J. Opt. Soc. Am. B* **36**, 2414–2422 (2019).
190. Lipovšek, B., Krč, J. & Topič, M. Optimization of microtextured light-management films for enhanced light trapping in organic solar cells under perpendicular and oblique illumination conditions. *IEEE J. Photovolt.* **4**, 639–646 (2014).
191. Eisenhauer, D., Trinh, C. T., Amkreutz, D. & Becker, C. Light management in crystalline silicon thin-film solar cells with imprint-textured glass superstrate. *Sol. Energy Mater. Sol. Cells* **200**, 109928 (2019).
192. Kosten, E. D., Kayes, B. M. & Atwater, H. A. Experimental demonstration of enhanced photon recycling in angle-restricted GaAs solar cells. *Energy Environ. Sci.* **7**, 1907–1912 (2014).
193. Kosten, E. D., Newman, B. K., Lloyd, J. V., Polman, A. & Atwater, H. Limiting light escape angle in silicon photovoltaics: ideal and realistic cells. *IEEE J. Photovolt.* **5**, 61–69 (2015).


## Acknowledgements

The work by A.C. and S.C. was supported in part by the French ANR projects ULTRACIS-M under grant ANR-12-PRGE-0003, NATHISOL under grant ANR-12-PRGE-0004, NANOCELL under grant ANR-RF-2015-01, ICEMAN under grant ANR-19-CE05-0019, by the 'Programme d'Investissement d'Avenir' ANR-IEED-002-01 and by the H2020 project ARCIGS-M funded by the European Commission under grant 720887.

## Competing interests

The authors declare no competing interests.

## Additional information

**Supplementary information** is available for this paper at https://doi.org/10.1038/s41560-020-00714-4.

**Correspondence** should be addressed to S.C.

**Reprints and permissions information** is available at www.nature.com/reprints.

**Publisher's note** Springer Nature remains neutral with regard to jurisdictional claims in published maps and institutional affiliations.